Journal Pre-proofs

Theoretical and experimental studies on large deflection analysis of double corrugated cantilever structures

Deepak Kumar, Shaikh Faruque Ali, A. Arockiarajan

PII: S0020-7683(21)00216-X
DOI: https://doi.org/10.1016/j.ijsolstr.2021.111126
Reference: SAS 111126

To appear in: *International Journal of Solids and Structures*

Please cite this article as: Kumar, D., Ali, S.F., Arockiarajan, A., Theoretical and experimental studies on large deflection analysis of double corrugated cantilever structures, *International Journal of Solids and Structures* (2021), doi: https://doi.org/10.1016/j.ijsolstr.2021.111126

Theoretical and experimental studies on large deflection analysis of double corrugated cantilever structures

Deepak Kumar, Shaikh Faruque Ali, A. Arockiarajan*

Department of Applied Mechanics, Indian Institute of Technology Madras, Chennai - 600036, India.

Abstract

Corrugated structures are made up of panels with periodic profiles. These are used as a compliant mechanism and as core in sandwich plates for their direction dependent stiffness. Modeling and large deflection analysis of corrugated structure play an essential role in their design and application. This work proposes an iterative scheme for the large deflection analysis of double corrugated cantilever structures subjected to end point loads and uniformly varying load using a chain algorithm. The double corrugated structure is modeled by discretizing it into several basic corrugated units. Each basic unit is then split into two halves, and a solution is arrived at using an error minimization. The deflection of each of the halves is obtained, discretizing it into beam elements. Finally, the deflection of the double corrugated structure is calculated by assembling the deflection of each of the basic corrugated units. Furthermore, prototypes of the double corrugated structure are fabricated using aluminum sheets, and a moment actuation test is performed. The deflections of these prototypes obtained using the proposed iterative scheme are compared with ABAQUS® and validated with experiments, and the results are found to be in good agreement. An example problem is also solved, demonstrating the practical application of the proposed iterative scheme in the design of a double corrugated variable camber morphing wing with aerodynamic load actuated by the tendon-pulley system.

Keywords: Double corrugated structure, large deflection, nonlinear analysis, chain algorithm.

*Corresponding author

Email address: aarajan@iitm.ac.in (A. Arockiarajan)

1. Introduction

For a long time, corrugation has been seen as a simple and effective method of forming flexible and lightweight structures with high anisotropic behaviour, buckling load stability and energy absorbing capacity. It has been used in a wide range of engineering applications. Numerous innovative improvements in corrugated structures have taken place in recent years, involving more intricate and ingenious corrugation geometries and a combination of corrugations with advanced materials [1–4]. There are mainly two kinds of corrugated structures reported in literature, *i,e.* single corrugated structures and double corrugated structures for structural and aerospace applications [5–9].

In structural engineering applications, single corrugated plates have been widely used as shear walls in multi-storied or high-rise buildings. In recent years, single corrugated plate shear walls are designed towards a higher load-resistant [10–13]. However, the shear resistance of the conventional single corrugated plate shear walls is limited [14]. To meet the requirements of large shear resistance, a double corrugated plate shear walls have been designed [15]. Double corrugated plate shear walls are composed of two single corrugated plates that are symmetrically installed and assembled using connecting bolts.

In aerospace engineering, research on morphing wings has gained significant interest in recent years, due to their better aerodynamic efficiency and performance. Performance enhancement is possible by changing the wing shapes at different flight conditions [16]. Due to their axial compliance and orthotropic properties, corrugated structures represent a fascinating morphing wing solution [17]. These structures have been used as both morphing wing core structures and morphing skins as well [18, 19]. Single corrugated composite sheets were firstly proposed for flexible wing skins applications [17]. But one major drawback of corrugated skins is the potential increase in the aerodynamic drag. The skin drag can be reduced with the use of a discontinuous segmented skin and single corrugated core coated with an elastomer [19, 20]. Previtali et al. [21] proposed a new type of corrugation, called double-walled corrugated structure (DCo), which can be considered as a combination of two rectangular corrugation, one inside the other. The results reported that the DCo allows achieving higher axial compliance while retaining a high flexural rigidity, both un-

der tension and compression loads. Due to this, it can be considered as a promising morphing skin concept representing a possible solution to the previously described limitations of conventional single corrugations. Yokozeki et al. [18] developed a trailing edge (TE) morphing wing using a single corrugated structure as the core structure. The wind tunnel tests show that the morphing wing was superior to the conventional wing with hinged control surfaces. A framework to analyse single corrugated structure using nonlinear mechanics has been reported in Kumar et al. [8]. Experiments were also reported that matches well with the analytical framework. Kumar et al. [7] also introduced a variable camber morphing configuration with a double corrugated structure as the core. The proposed double corrugated structure is composed of two single corrugations that are symmetrically placed one over the other. The results show that the variable camber morphing configuration with double corrugated structure can take larger loads without severe deformation resulting in higher aerodynamic efficiency than the other available configurations.

Numerous studies have also investigated the mechanical behavior of single corrugated structures using analytical models, finite element analysis, and experimental approaches [22–26]. Still, very few studies have presented double corrugated structure. Tong et al. [14] presented the elastic buckling behavior of trapezoidal double corrugation shear wall subjected to pure in-plane shear loads. The double corrugation shear wall is modeled as an orthotropic plate, and the rigidity constants are compared with finite element (FE) analyses. Further theoretically, Tong et al. [27] investigated the shear resistant behavior of the double corrugation shear wall through monotonic shear tests and finite element analysis. Previtali et al. [28] reported bending and axial stiffness of the double-walled corrugated structure (DCo) using a finite element model. It is shown that the bending stiffness depends nonlinearly on the applied moment. Experimental tests confirm the numerically predicted performance. From the literature, a need for a nonlinear model for double corrugated structure is identified. The model should be able to pick up nonliniarity due to large deflection in the design for example in morphing wing application. Although the deflection of the double corrugated structure can be calculated using the finite element method. But for detailed modelling and design of the structure will lead to a high computational cost, which also encourages the study of analytical based models.

In this paper, an iterative scheme is developed to analyze double corrugated structure. The

model is derived using Euler-Bernoulli beam theory considering geometric nonlinearity. The proposed model is used to calculate large deflection of a double corrugated cantilever structure under the action end point load and uniformly varying load. Large deflections of a basic corrugated unit and the double corrugated structure with cantilever boundary condition are investigated using nonlinear shooting method integrated to a chain algorithm. Results of the analytical method are compared with ABAQUS® simulations and validated using experiments. Sections 2 and 3 give the formulation of the proposed iterative scheme developed for the double corrugated structure for end point loads and uniformly varying load, respectively. In Section 4, study on the effect of rivets layout on the structure has been presented. Section 5 provides the details of the experimental setup. In Section 6, results from iterative scheme and ABAQUS® simulations are compared with the experiments for the double corrugated structure. In addition, the results included the practical application of the proposed method to the design of a double corrugated morphing wing. In Section 7, the current work has been summarized and conclusions are drawn based on the analytical, numerical and experimental studies.

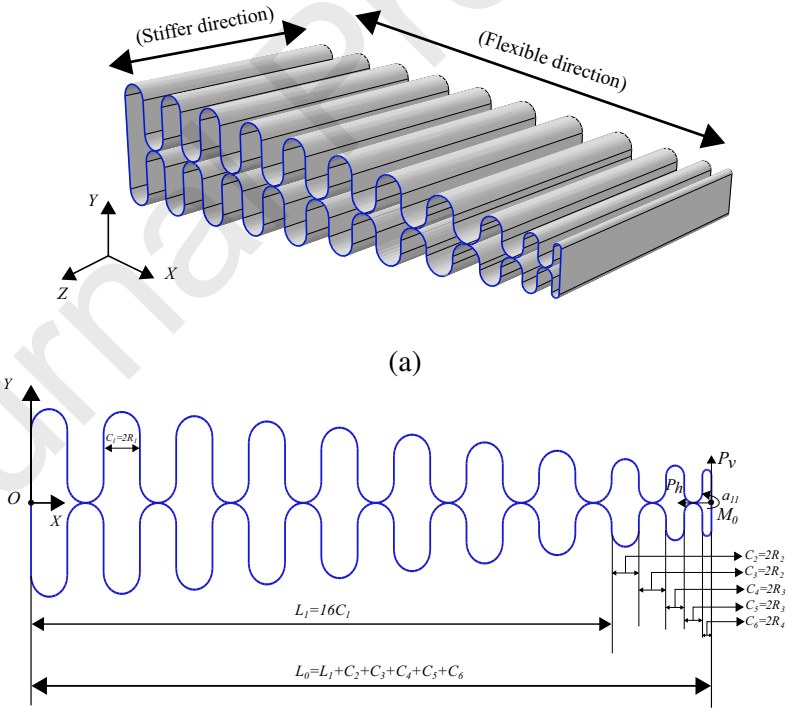

Figure 1: Schematic of the double corrugated structure used in this study. (a) Double corrugated structure with anisotropy, (b) projection of the structure in *X*-*Y* plane with variable spacing, end loads and boundary conditions

2. Large deflection analysis of double corrugated structures with end loads

In this section, the mathematical formulation of a double corrugated structure under the action of free end loads is presented. The double corrugated structure considered in this study is composed of two single corrugations as shown in Fig. 1(a). The structure is uniform along Z direction and the corrugation is along X-Y plane. Hence, a two dimensional model (plane stress) as shown in Fig. 1(b) is considered for the analysis. The structure is fixed at the end O and loads are applied at the free end a_{11}. The direction of forces and moment as shown in Fig. 1(b) are assumed to be positive. Geometrical and material parameters considered for the analysis are given in Table 1.

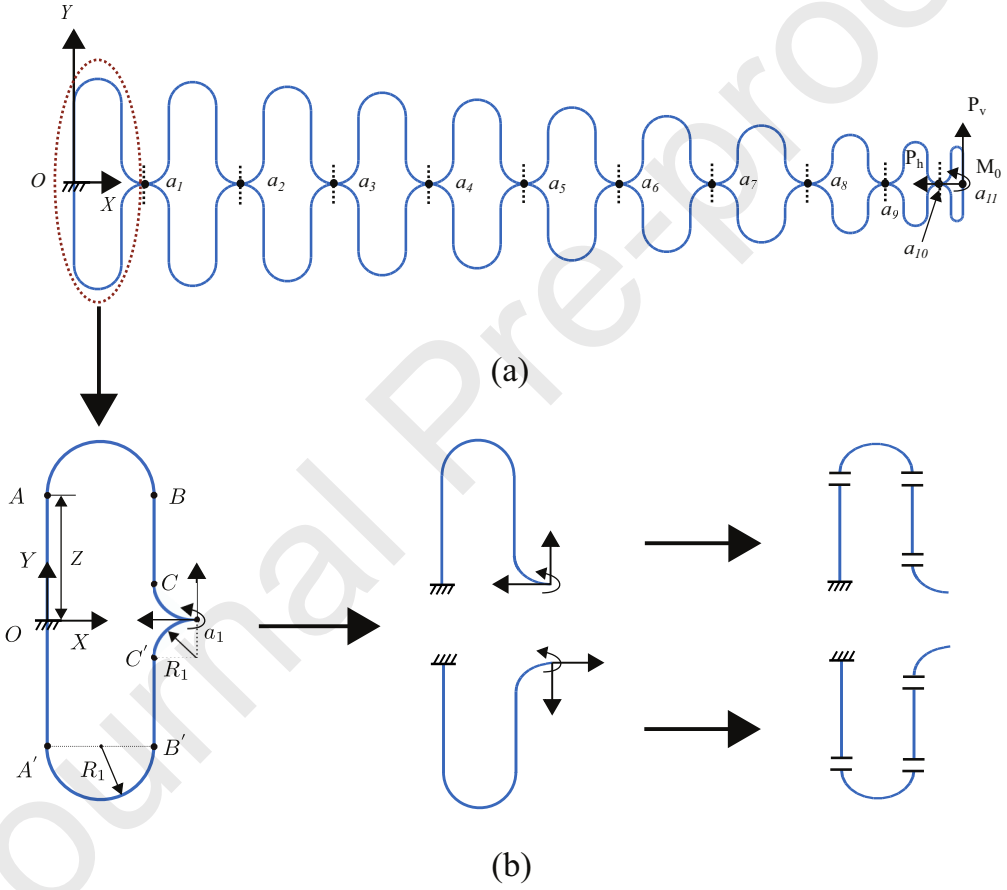

Figure 2: Geometry of double corrugated structure. (a) Double corrugated structure consisting of 11 basic units, (b) shows a basic unit and split of basic unit into top and bottom halves which are further discretized into beams. Proper compatibility conditions are enforced during the solution process.

As shown in Fig. 2, the double corrugated structure is made of basic corrugated units which can be of same or different sizes. In this work, we considered different sizes of corrugation unit

(see Fig. 2(a)). The basic analysis remains same and can be extended to a special case of same sized corrugation unit. The structure is divided into 11 basic corrugated units. Basic corrugated units (as shown in Fig. 2(b)) are repeated to generate the double corrugated structure. As shown in Fig. 2(b), each basic corrugated unit is split in to two, *i.e.*, top and bottom open chain units. Each open chain unit is further divided into multiple straight, semi-circular and quarter-circular segments. The deflection of the top and bottom open chain units are determined using a chain algorithm [29]. The process is explained in detail in subsection 2.1. An analytical formulation for large deflection analysis of the double corrugated structure is attempted through the understanding of load-deformation analysis of the basic corrugated unit. The study is then extended to the complete structure taking appropriate care of continuity conditions at the joints (namely at $a_1, \ldots, a_{11}$ in Fig. 2(a)). Deflection of the double corrugated structure is calculated by combining the deflections of each unit appropriately.

This section is divided into four subsections. Subsection 2.1 gives a description of the geometry and free body diagrams of the basic units of double corrugated structure. The second and third subsections outline a solution scheme (chain algorithm) to obtain the deflected profile of basic unit and the double corrugated structure respectively. In the fourth subsection, the proposed algorithm is summarized as applicable for the total structure with the help of a flow chart.

Table 1: Geometrical parameters of the double corrugated structure made of aluminum

Parameter	Value
L_0	150 mm
L_1	128 mm
Z	12.73 mm
R_1	4 mm
R_2	3 mm
R_3	2 mm
R_4	1 mm
Width (b)	75 mm
Sheet thickness (t_{cs})	0.5 mm
Modulus of elasticity of aluminum (E)	70 GPa

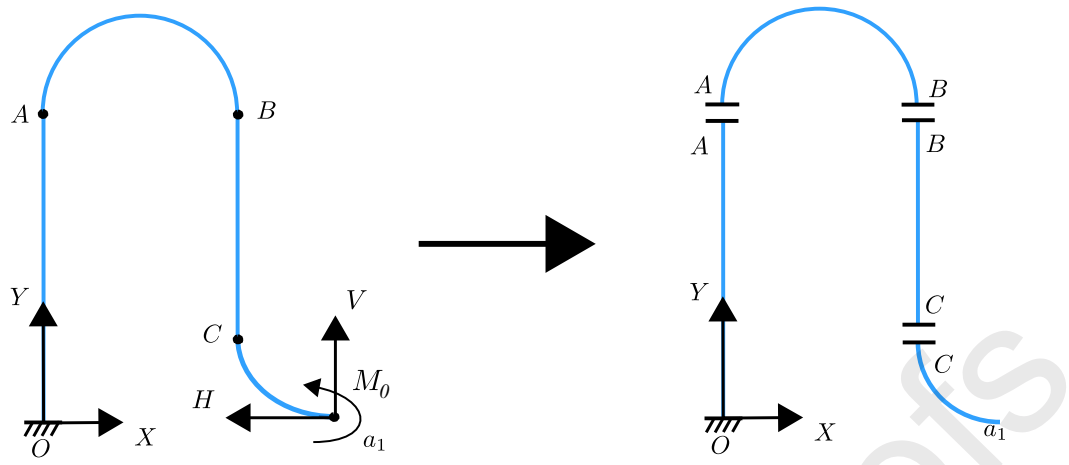

Figure 3: Open chain unit with applied loads and moment at free end (H = 50 N, V = 50 N and M_0 = 1000 N-mm). It is split into 4 beams.

2.1. Large deflection analysis of a open chain unit using chain algorithm

In this subsection, the chain algorithm is described as a numerical procedure to cope with the geometric nonlinearity in open chain unit. The chain algorithm exploits the moment distribution generated by any triplets of external loads, namely axial/transverse loads and moment (H, V, M_0). The end O of the open chain unit is fixed and loads are applied at the free end a_1 (H = 50 N, V = 50 N and M_0 = 1000 N-mm). The open chain unit is then divided into two straight (OA, BC) and two curved beams (AB, Ca_1) as shown in Fig. 3. Each beam is treated as a cantilever which is fixed to the end of the previous beam. The slope and deflection of the free end of the previous beam are considered as rigid body motions at the fixed end of the following beam. The displacement of each beam member is then determined using the Euler-Bernoulli beam theory considering large deflections (geometric nonlinearity) [30]. Fig. 4 shows the flowchart for determining the deflection of the basic corrugated unit.

The chain algorithm does not yield correct solution after first iteration, owing to the nonlinear moment-curvature relation. Therefore the moments acting on the various elements of the structure must be calculated from the previous deformed state. It is thus necessary to iteratively update the moment with respect to the deformed state until convergence is attained between the successive deformed states.

The moment M_j^i at i^{th} node of the structure and for the j^{th} iteration is calculated as,

$$M_j^i = M_0 + [V(x_j^{a_1} - x_j^i) - H(y_j^{a_1} - y_j^i)] \qquad i = A, B, C, ..., a_1; \quad j = 1, 2, ..., n_1 \tag{1}$$

where x_j^i and y_j^i are coordinates of i^{th} node of the open chain unit at j^{th} iteration and n_1 denotes the number of iterations.

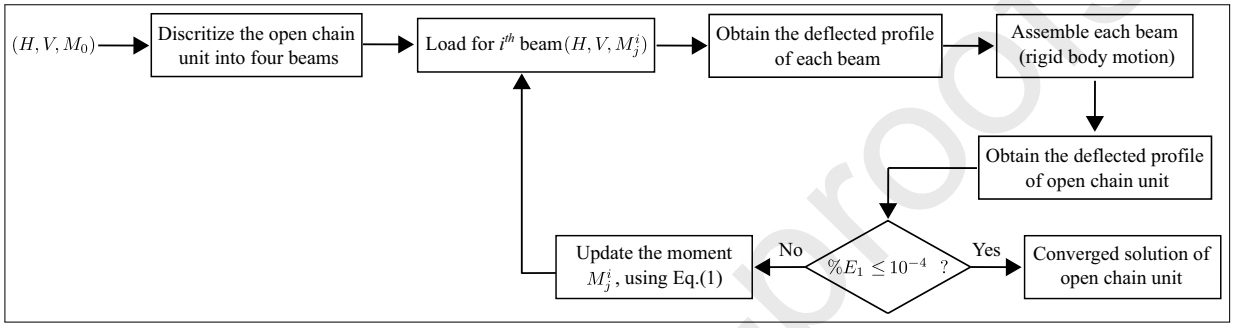

Figure 4: Flow chart to obtain the deflected profile of an open chain unit.

The chain algorithm, described in Fig. 4, proceeds as follows:

- *Iteration* 1: The initial moment M_0^i generated by the external forces and moment is applied to the undeformed state of the open structure. The deformed shape $\delta_1(j = 1)$ is obtained after the application of M_0^i.
- *Iteration* 2: The moment distribution M_1^i is derived from the deformed shape $\delta_1(j = 1)$. The new deformed shape $\delta_2(j = 2)$ is obtained through the application of M_1^i.
- *Iteration j*: The j^{th} moment distribution M_j^i as given by Eq. (1) is applied to deformed shape δ_j to determine the deformed state corresponding to the $(j + 1)^{th}$ iteration.

Iterations continue until a convergence is achieved according to a criterion (Eq. (2)). When the error percentage, E_1, in the magnitude of tip displacement (U) between two successive iterations is less than $10^{-4}\%$ iterations are stopped. As it can be noted in Fig. 5(a), the convergence is obtained

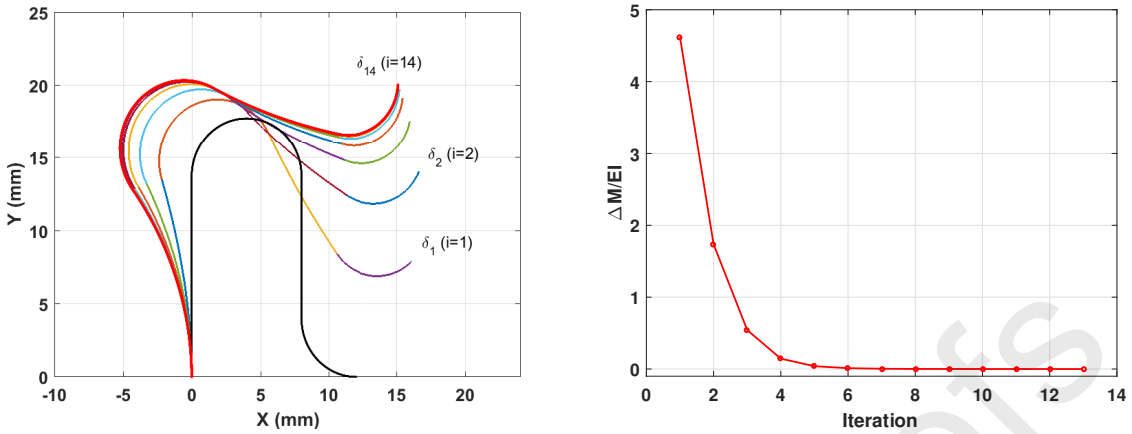

(a) (b)

Figure 5: Application of the chain algorithm to open structure (a) deformed shapes δ_i of open structure with every iteration i, (b) the moment variation ΔM^C for the node C.

within 14 iterations.

$$E_1 = \frac{|U_j^{a_1} - U_{j-1}^{a_1}|}{U_j^{a_1}} \times 100\%, \qquad \text{where} \quad U_j^{a_1} = \sqrt{(x_j^{a_1})^2 + (y_j^{a_1})^2} \tag{2}$$

Reporting the variation of the moment $\Delta M_j^i = M_j^i - M_{j-1}^i$, we obtain the plot reported in Fig. 5(b) for the node C. As specified previously, the value of ΔM^C also converges within 14 iterations.

2.2. *Solution scheme for large deflection of the basic corrugated unit*

The basic corrugated unit as shown in Fig. 6 is split in to two open chain units. The applied loads (H, V, M_0) are shared between the two such that equilibrium is satisfied at the free end (see Fig. 6). The deflections of the top and bottom open chain units are obtained using the flowchart shown in Fig. 4. There are three unknown variables (F_h, F_v, p) to be determined. The variables are determined such that the free end of the top and bottom open chain unit move together which implies the free end coordinates and angles $[(x_t, y_t, t_t)\ (x_b, y_b, t_b)]$ should be equal. An error metric, E_D, is defined as a function of the end coordinates of the deflected profiles of the top and bottom sections as shown below.

$$E_D(F_h, F_v, p) = \sqrt{(x_t - x_b)^2 + (y_t - y_b)^2 + (t_t - t_b)^2} \tag{3}$$

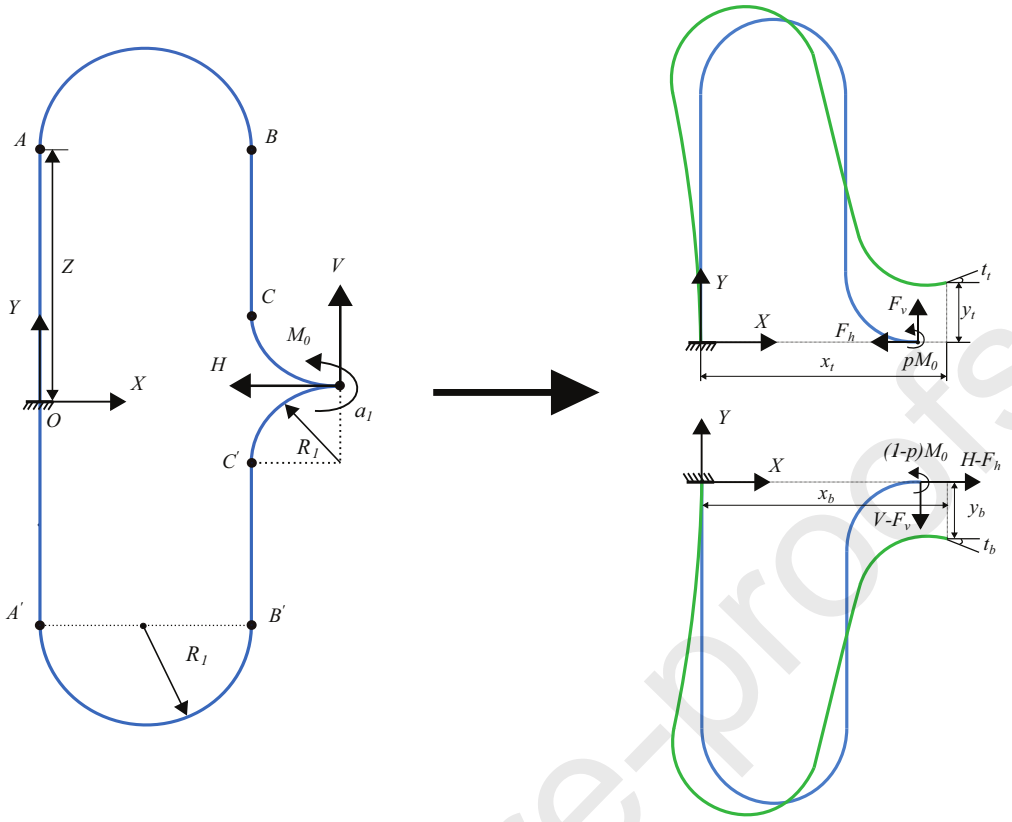

Figure 6: Basic corrugated unit subjected to end forces and an end moment. It is split into two open chain units.

where (x_t, y_t, t_t) are the end point coordinates and tip angle of the top open chain unit and (x_b, y_b, t_b) are of the bottom open chain unit (see Fig. 6).

In order to solve this problem we need to minimize E_D given in Eq. (3). The minimization problem is described by the following equation

$$\begin{aligned} \min \quad & E_D(F_h, F_v, p) \qquad (F_h, F_v, p) \in R \\ \text{s.t.} \quad & x_b - x_t = 0, \\ & y_b - y_t = 0, \\ & t_b - t_t = 0 \end{aligned} \tag{4}$$

To solve the above minimization problem the *fmincon*() function is used from the MATLAB® Optimization Toolbox [31], by taking into account the constraints of the problem, as stated in

Eq. (4). The optimum values $F_{opt,h}$, $F_{opt,v}$, p_{opt} obtained by solving Eq. (4) are used to obtain the deflected profile of the basic corrugated unit for the given loading conditions (H, V, M_0). Figure 7 shows the flowchart for determining the deflection of the basic corrugated unit for the given input loads (H, V, M_0).

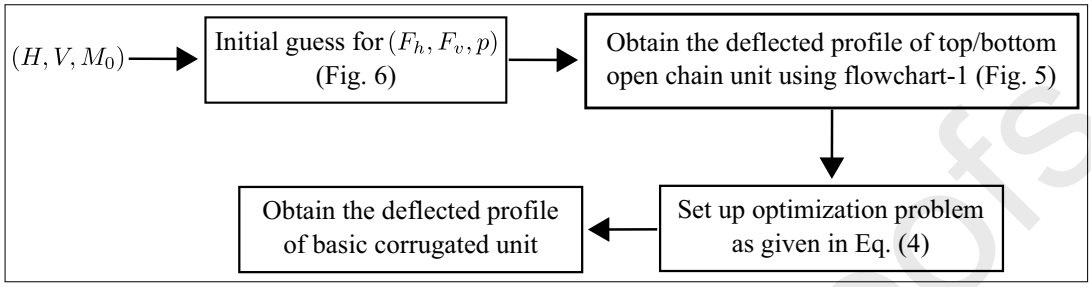

Figure 7: Flow chart to obtain the deflected profile of a basic corrugated unit.

Sensitivity of initial guess and bounds on minimization function:

The sensitivity of initial guess in solving the basic corrugated unit is studied using the Block Classification pre-search technique [32]. In this technique, the search space for the *fmincon*() function used in the iterative scheme can be reduced to a set of potential subspaces, Ω which is likely to contain the global minima. The technique is explained through the following steps:

Step 1: An initial search space, α_0 with bounds wide enough to contain the global minima is chosen based on the applied loads and physical constraints of the problem.

Step 2: The error function, E_D is evaluated at the points, $X_i's$, (F_h, F_v, p) contained in α_0.

Step 3: In order to find the potential subspaces, Ω, a virtual threshold error function value, E_D^* is chosen between the minimum and maximum error function values calculated in step 2. The potential subspaces are identified from α_0 based on the condition,

$$\Omega : E_D(X) \leq E_D^*, X \in \alpha_0 \tag{5}$$

Step 4: A set of initial guesses, $X_{0,i}$ ($i = 1, 2, ...n, n =$ number of initial guesses) which have the least error function values are chosen from the potential subspace and are used in the global optimization function *fmincon*(). The initial guess from this set which takes the least computation time is taken to be the optimal one.

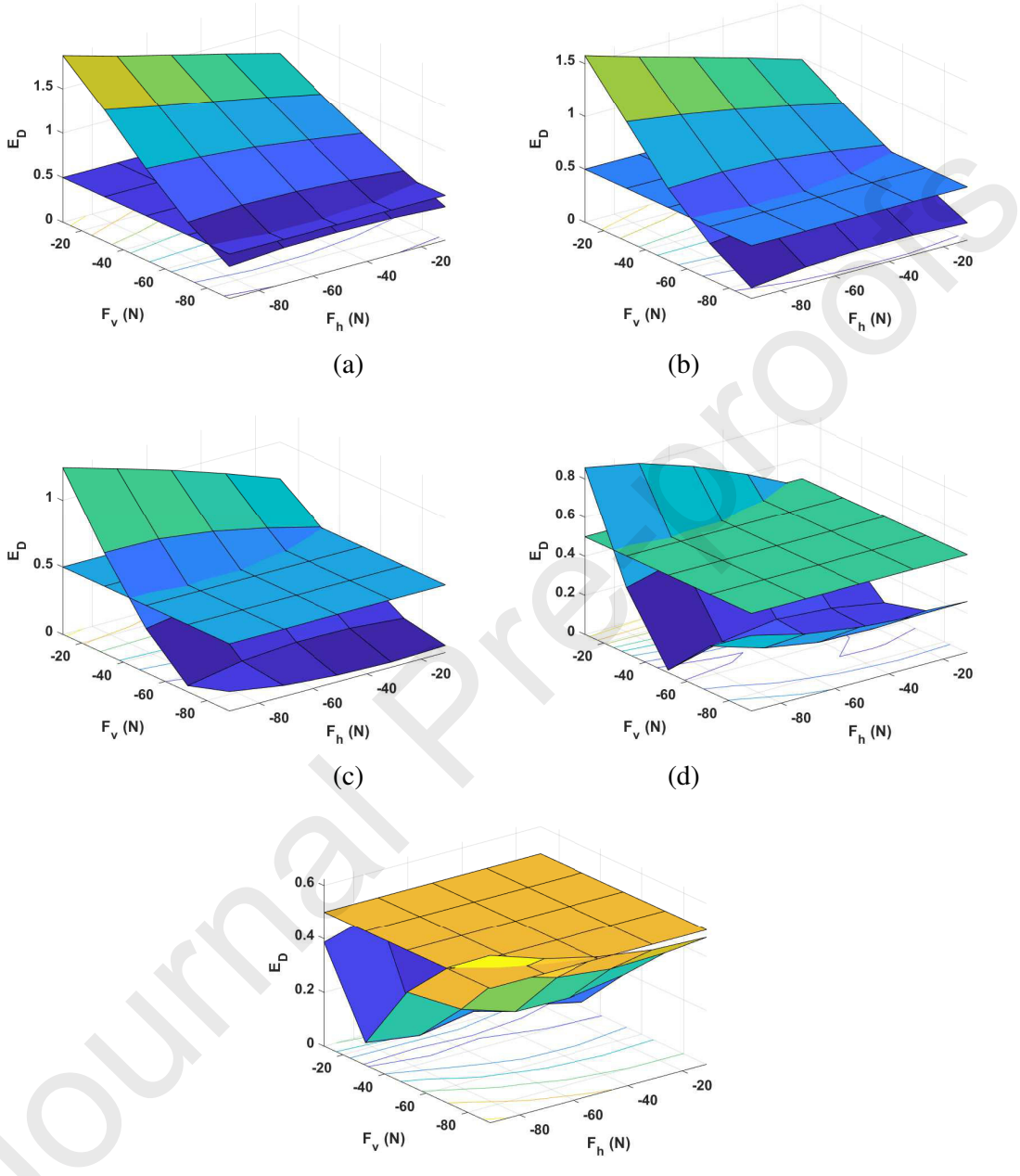

Figure 8: Surface plots for different p values to evaluate potential subspaces, with virtual threshold plotted as $E_D^* = 0.5$ and applied end loads, $M_0 = -1000$ N-mm, $P_h = -50$ N, $P_v = -75$ N (a) $p = 0.1$, (b) $p = 0.3$, (c) $p = 0.5$, (d) $p = 0.7$ and (e) $p = 0.9$.

Table 2: Candidate initial guesses from surface plots

S. No.	Potential subspace				Initial Guesses		
	F_h (N)	F_v (N)	p	Min. E_D	F_h (N)	F_v (N)	p
1	[-90,-10]	[-90,-78]	0.1	0.3604	-90	-90	0.1
2	[-90,-10]	[-90,-55]	0.3	0.1028	-90	-90	0.3
3	[-90,-10]	[-90,-31]	0.5	0.0369	-31	-90	0.5
4	[-90,-10]	[-90,-10]	0.7	0.0139	-90	-51	0.7
5	[-90,-10]	[-90,-10]	0.9	0.0155	-11	-31	0.9

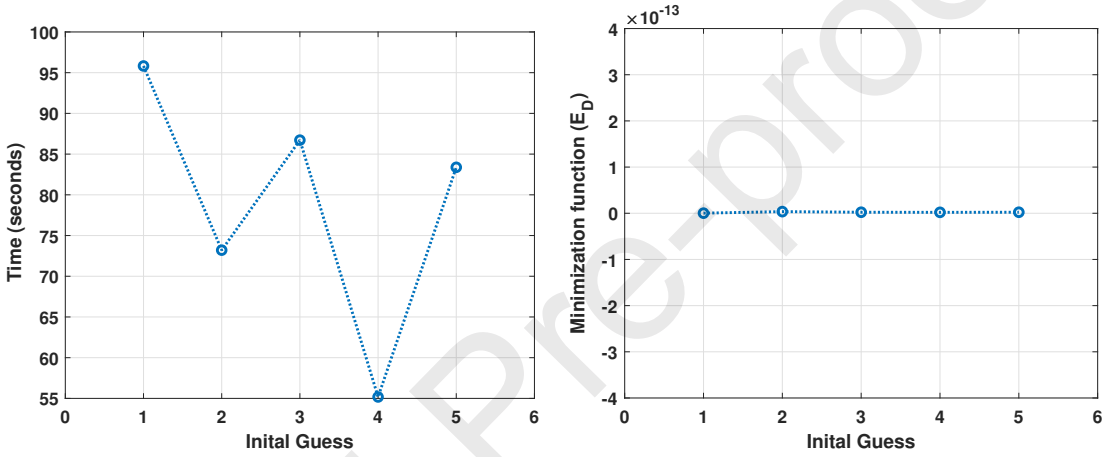

(a) (b)

Figure 9: Effect of initial guess on (a) Computational time, (b) Minimization function E_D.

In our case, for the initial search space, α_0, bounds for p, F_h and F_v are chosen as $[0.1, 0.9]$, $[-90N, -10N]$ and $[-90N, -10N]$ respectively. Fig 8 shows the error function evaluations at all p, F_h and F_v combinations within these bounds, with the virtual threshold of the error function taken as $E_D^* = 0.5$. The p, F_h and F_v combinations which satisfy the condition given in Eq. 5 and having the least error function value corresponding to each p value are taken as candidate initial guesses to study their sensitivity on computation time and accuracy (See Table 2). From Fig. 9 (a) it can be seen that initial guess 4 corresponding to the least value of E_D (See Table 2) has the smallest computation time. For the given end loads this initial guess is used to solve the first basic corrugated unit in the double corrugated structure and the solution of this unit is taken as the initial guess for the next unit. Similarly the initial guess for the subsequent basic units are taken from their

predecessor's solution. Fig. 9 (b) shows that the accuracy of the iterative scheme is independent of initial guess.

The effect of bounds in *fmincon*() function, for solving a basic corrugated unit (End loads: $P_h = 50$ N, $P_v = 50$ N, $M_0 = 1000$ N-mm), on computation time and accuracy are studied for six different bound cases as shown in Table 3. From Figs. 10 (a) and (b) it can be seen that the maximum difference between the computational time taken is less than $1s$ and the minimization function value remains constant. This implies that bounds have negligible influence on computation time and accuracy for our problem. Hence, in our case we have not specified any bounds for solving.

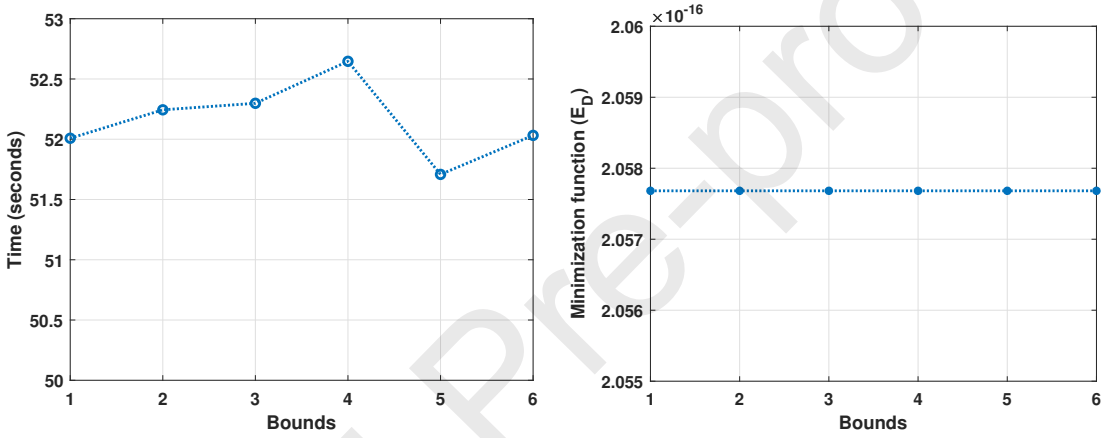

(a) (b)

Figure 10: Effect of bounds in minimization problem on (a) Computational time, (b) Minimization function E_D.

Table 3: Lower and upper bounds for sensitivity study

Bound cases	Lower Bound			Upper bound		
	F_h (N)	F_v (N)	p	F_h (N)	F_v (N)	p
1.	No	bounds		No	bounds	
2.	0	0	0	5000	5000	1
3.	0	0	0	2000	2000	1
4.	0	0	0	1000	1000	1
5.	0	0	0	500	500	1
6.	0	0	0	100	100	1

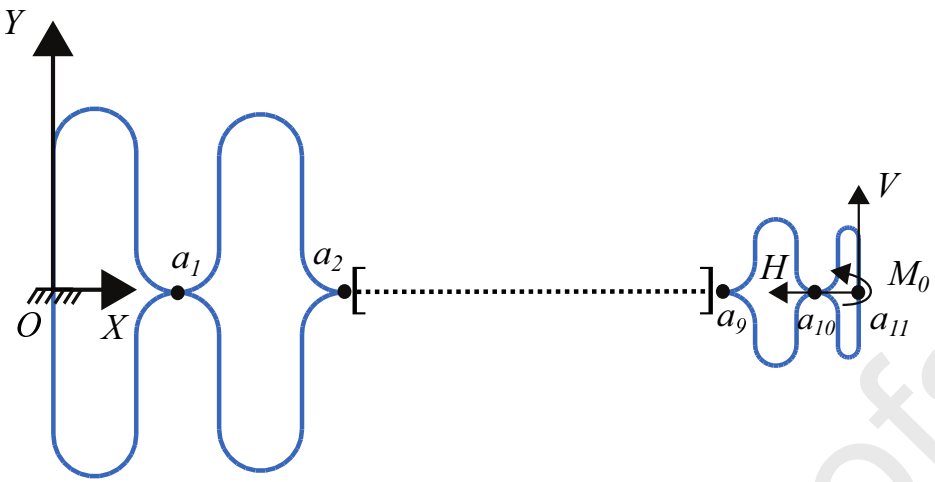

Figure 11: Double corrugated structure divided in to 11 basic units.

2.3. *Solution scheme for large deflection of the double corrugated structure*

The deflected shape of the double corrugated structure is obtained using a chain algorithm. The structure is divided into N corrugated units, here $N = 11$ as shown in Fig. 11. The deflected profile of each corrugated unit is obtained using the flowchart shown in Fig. 7. The moment at free end of the i^{th} corrugated unit is given by

$$M_j^i = M_0 + [V(x_j^{a_{11}} - x_i^i) + H(y_i^{a_{11}} - y_i^k)] \qquad i = a_1, a_2, ..., a_{11}; \quad j = 1, 2, ..., n_2 \tag{6}$$

where x_j^i and y_j^i are coordinates at the free end of i^{th} corrugated unit at j^{th} iteration and n_2 denotes the number of iterations.

The deflected profile of the double corrugated structure is obtained by combining the deflected shapes of each of the units keeping continuity conditions at the joints intact. Figure 12 shows the flowchart for determining the deflection of the double corrugated structure. The convergence is achieved when the error percentage, E_2, (Eq. (7)) in the magnitude of tip displacement (U) between two successive iterations is less than $10^{-4}\%$.

$$E_2 = \frac{|U_j^{a_{11}} - U_{j-1}^{a_{11}}|}{U_j^{a_{11}}} \times 100\%, \qquad \text{where} \quad U_j^{a_{11}} = \sqrt{(x_j^{a_{11}})^2 + (y_j^{a_{11}})^2} \tag{7}$$

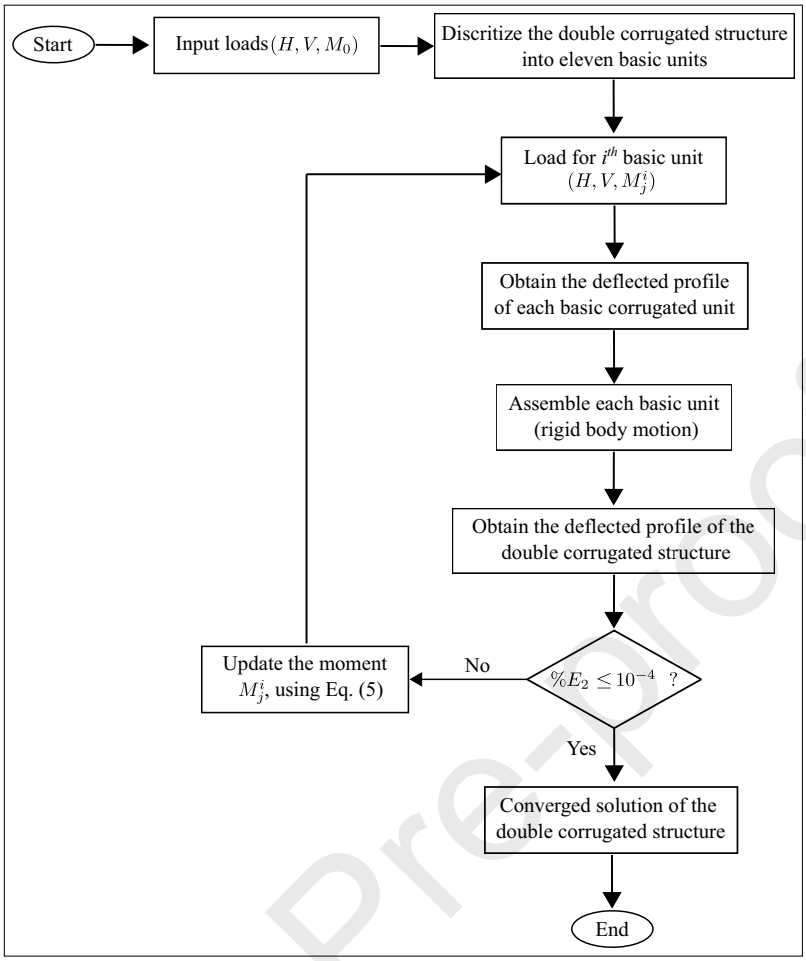

Figure 12: Flow chart to obtain the deflected profile of the double corrugated structure.

2.4. Summary of the algorithm for large deflection analysis of the double corrugated structure

In this subsection, a summary of the algorithms described in Subsections 2.1, 2.2 and 2.3 is presented for the large deflection analysis of the double corrugated structure for given free end loads (P_h, P_v, M_0) as shown in Fig. 2(a). To better clarify the proposed algorithm, the logic is described through flowcharts as shown in Figs. 13(a), (b) and (c). The double corrugated structure is first divided into $N = 11$ basic corrugated units. The moment at i^{th} basic corrugated unit for j^{th} iteration is calculated as

$$M_j^i = M_0 + [P_v(x_j^{a_{11}} - x_j^i) + P_h(y_j^{a_{11}} - y_j^i)] \qquad i = a_1, a_2, ..., a_{11}; \;\; j = 1, 2, ..., n_3 \tag{8}$$

where x_j^i and y_j^i are free end coordinates of i^{th} corrugated unit at j^{th} iteration and n_3 denotes the number of iterations.

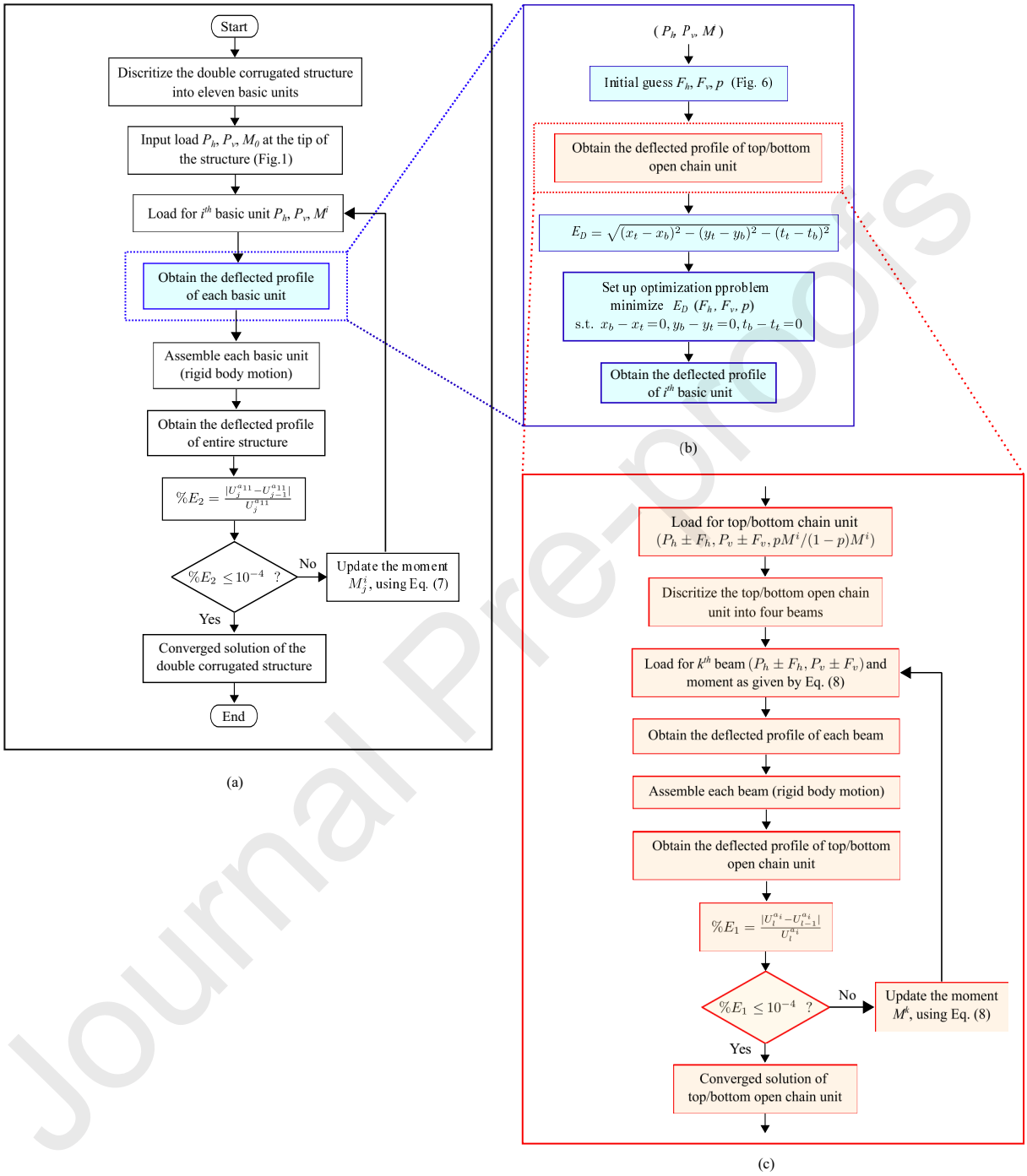

Figure 13: Illustration of proposed method using flow charts, (a) flow chart for calculating the deflection of double corrugated structure, (b) internal loop: flow chart to obtain the deflected profile of corrugated unit, (c) chain algorithm for both the top/bottom half.

The basic corrugated unit is then further split into two, *i.e*, top and bottom open chain units. Each corrugated unit is subjected to an end load (P_h, P_v, M_j^i). The applied moment M_j^i at i^{th} basic corrugated unit and for j^{th} iteration is spilt in the ratio of p and $(1-p)$ between the top and bottom open chain units. Force balance between the top and bottom open chain units is ensured by equal and opposite forces, F_h and F_v in the horizontal and vertical directions respectively. The top and bottom open chain units are thus subjected to loads $(P_h \pm F_h, P_v \pm F_v, pM_j^i/(1-p)M_j^i)$. Each open chain unit is further subdivided into straight beams (OA; BC in the top and OA', BC' in the bottom open chain units) and curved beams (AB, Ca_1 in the top and $A'B'$, $C'a_1$ in the bottom open chain units) of constant radius R_1. The moment at k^{th} node of the top and bottom open chain units for l^{th} iteration are calculated as

$$\begin{aligned} M_l^{k^t} &= pM_j^i + [P_v(x_l^{a_i} - x_l^{k^t}) + P_h(y_l^{a_i} - y_l^{k^t})] \qquad k^t = A, B, ..., Ca_1; \;\; l = 1, 2, ..., n_4 \\ M_l^{k^b} &= (1-p)M_j^i + [P_v(x_l^{a_i} - x_l^{k^b}) + P_h(y_l^{a_i} - y_l^{k^b})] \quad k^b = A', B', ..., C'a_1; \;\; l = 1, 2, ..., n_4 \end{aligned} \tag{9}$$

where $(x_l^{k^t}, y_l^{k^t})$ and $(x_l^{k^b}, y_l^{k^b})$ are free end coordinates of k^{th} node of the top and bottom open chain unit, respectively, at l^{th} iteration and n_4 denotes the number of iterations.

The flowchart shown in Fig. 13(c) depicts the logic of the chain algorithm for obtaining the deflected shapes of the top and bottom open chain units subjected to end loads of $(P_h + F_h, P_v + F_v, pM_j^i)$ and $(P_h - F_h, P_v - F_v, (1-p)M_j^i)$ respectively. For each node (free end of beam) and iteration, the bending moments are calculated using Eq. (9). The deflected profile of each beam is then obtained by means of the Euler-Bernoulli beam model. Then compatibility conditions are applied to the free end of every beam. This procedure is continued till the last beam is reached. The error is then calculated using Eq. (2) (as given in Subsection 2.1). The loop is terminated if this error is within the specified tolerance ($10^{-4}\%$). Otherwise the new moment calculated by Eq. (9) is in be applied to the next iteration.

The flowchart reported in Fig. 13(b) is for determination of the deflection of each corrugated unit. The input for this flowchart is the equivalent load from the first flow chart (P_h, P_v, M_j^i) (See Fig. 13(a)). For an initial guess of the unknown forces (F_h, F_v, p), the flowchart shown in Fig. 13(c) is evaluated to determine the deflection of the top and bottom open chain units. A minimiza-

tion problem with constraints described by Eq. (4) is set up and solved using *fmincon*() from the MATLAB® Optimization Toolbox (see subsection 2.2). The deflected profile is calculated using the optimal values ($F_{opt,h}$, $F_{opt,v}$, p_{opt}) of the unknown variables.

Deflected shape of the double corrugated structure is then obtained by combining the deflected shapes of each of the basic units keeping the continuity conditions at the joints intact. After obtaining the deflected profile of the structure, the convergence criterion given in Eq. (7) is checked (as given in subsection 2.3). If the convergence criterion is met, the loop is exited and the converged solution of the double corrugated structure is obtained. Otherwise the moment at each unit is updated as given by Eq. (8).

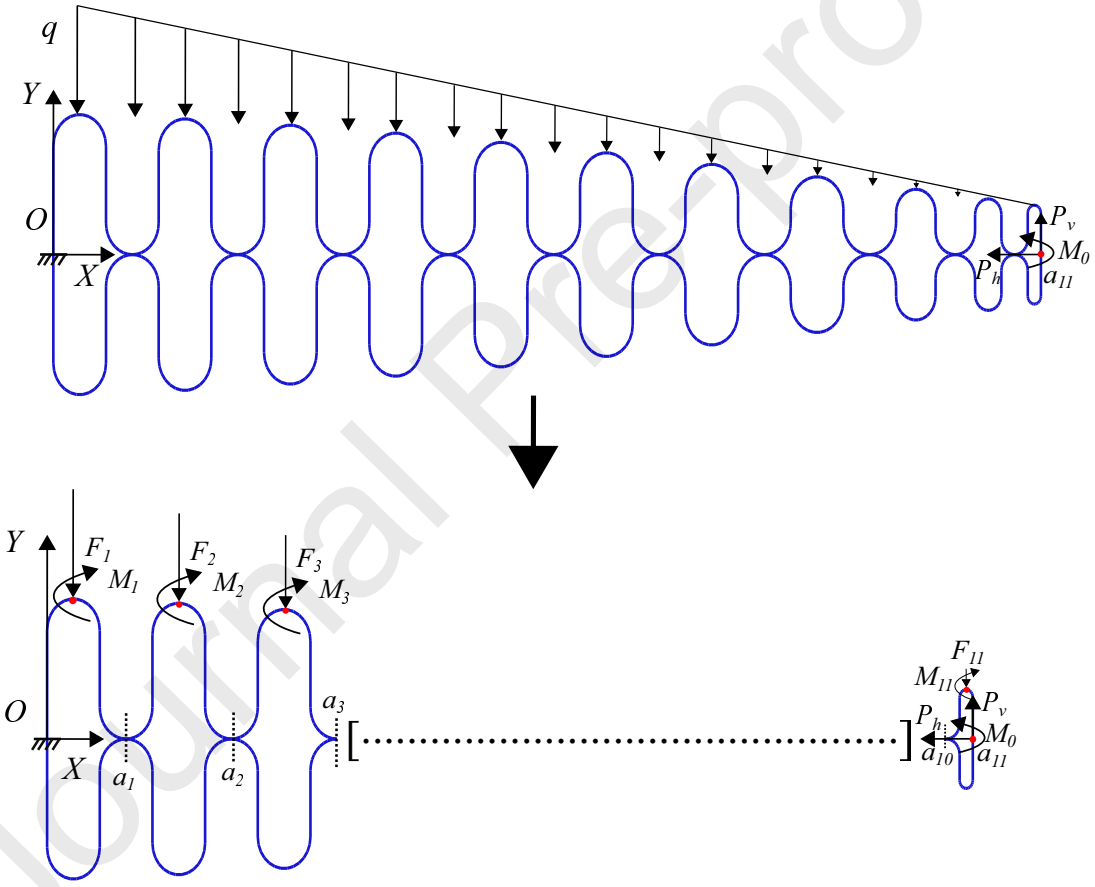

Figure 14: Schematic of the cantilever corrugated structure under the action of uniformly varying load and end point loads.

3. Double corrugated structure under uniformly varying (triangular distribution) load and end point loads

In this section, formulation for double corrugated structure subjected to a uniformly varying load and point loads at end a_{11} is presented with large deflection analysis. Figure 14 shows the double corrugated structure with end O fixed and subjected to uniformly varying load (peak value of q) and end point loads (P_h, P_v, M_0). The double corrugated structure shown in Fig. 14 is divided into 11 basic corrugated units. These units are considered to be cantilevered structure fixed to the end of the previous unit like a chain link. The uniformly varying load is resisted by the semicircular segments and load between two the gap of two semicircle segment is transferred to the previous semicircle. The equivalent load for the j^{th} unit is calculated by integrating force distribution between j^{th} and $(j+1)^{th}$ unit. This load is then transferred as force and moment (F_j, M_j) to the free end of the j^{th} unit. These equivalent loads ($F_1, M_1, F_2, M_2, ..., F_{11}, M_{11}$) due to the uniformly varying load are applied to semicircular segments (loads are applied at red dot on the semicircles) as shown in Fig. 14. The deflected profile of the double corrugated structure is obtained using the chain algorithm as explained in Section 2.

4. Effect of rivet layout on the structural behaviour of double corrugated structure

The double corrugated structure is assembled by placing two corrugated sheets one above the other and riveting them at some or all contact locations. In order to study the effect of rivet layout on the structural behaviour of the double corrugated structure modelled in ABAQUS®, we have chosen two different rivet layouts in the longitudinal direction, as shown in Fig. 15. In layout-1 riveting is done at all contact locations and in layout-2 alternative contact locations are riveted, as shown in Figs. 15(a) and (b) respectively. Since the sheet thickness is small compared to the rivet diameter, the rivets are considered to be stronger than the sheet in view of failure. The constraints produced by a rivet joint is idealized by rigidly constraining the nodes that are part of the sheet surface equal to the rivet area [33]. In our case we have accomplished this in ABAQUS® by connecting the two corrugated sheets at the rivet location using two rigid elements at a distance of 2mm apart equal to the rivet diameter, as shown in Fig. 15.

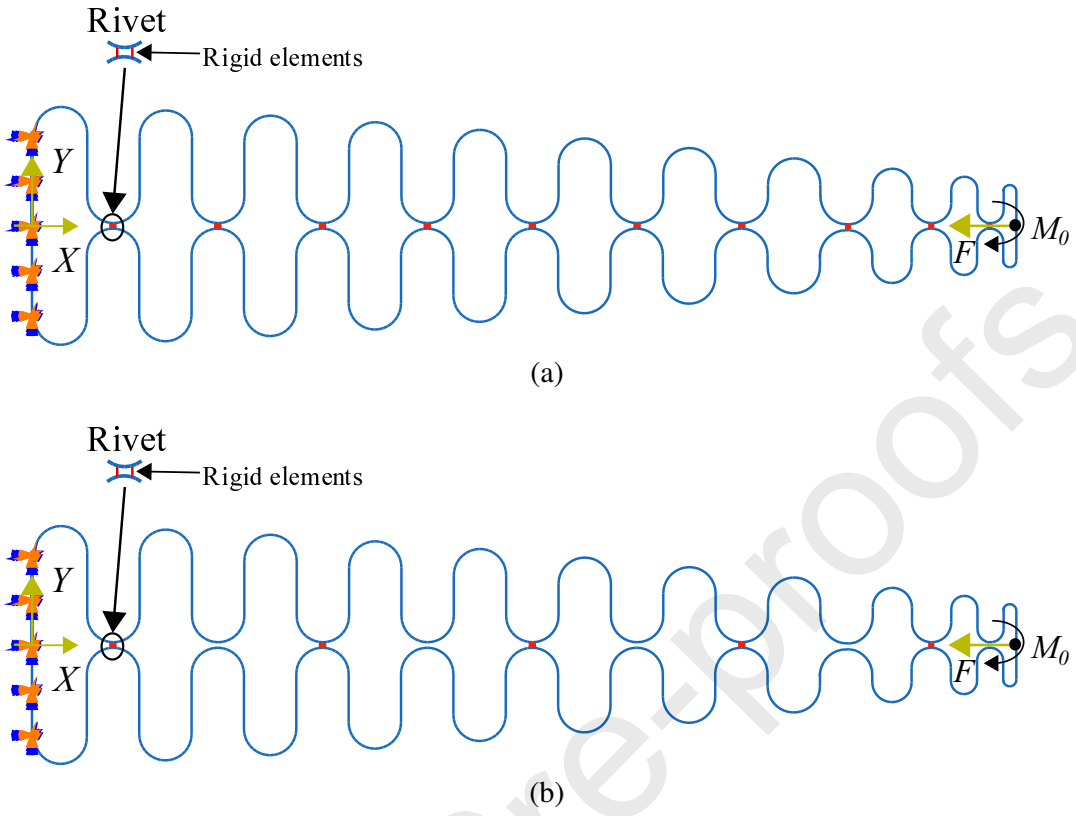

Figure 15: Double corrugated structure with different rivet layouts modelled using FEA in ABAQUS® (a) layout-1 and (b) layout-2.

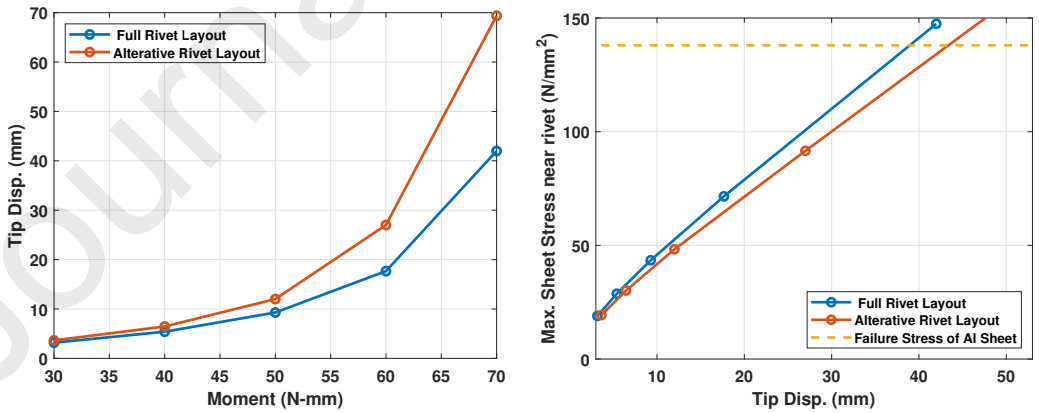

Figure 16: Effects of rivet layouts on structural behaviour of the double corrugated structure (a) Tip displacement against actuation moment, (b) Maximum stress developed in sheet near rivet joints against tip displacement.

Fig. 16 shows the effects of rivet layouts on structural behaviour of the double corrugated structure. Fig. 16 (a) shows the increased stiffness of layout-1 compared to layout-2 due to more number of rivet attachments. From Fig. 16 (b) it can be seen that for a particular tip displacement, the maximum stress developed in the sheet near rivet joints is more for layout-1 compared to layout-2. Also, considering the failure stress of the sheet to be 50 percent of the tensile strength of Aluminium, the sheet in layout-1 fails for a lesser tip displacement than the one in layout-2. Since layout-2 facilitates larger deflection than layout-1 without failure, it has been incorporated in the experimental prototype.

(a) (b)

Figure 17: Fabrication of double corrugated structure (a) mould of the corrugated structure, (b) prototype of double corrugated structure joined using rivets.

5. Experimental observation

To validate the proposed numerical scheme experiments are carried out on fabricated prototypes. The double corrugated structure is designed and fabricated using aluminum sheets. The mould used for the fabrication is shown in Fig. 17(a) which is prepared by steel blocks using a numerical control machine. The aluminum sheet is pressed between the moulds to make the prototype of the corrugated structure. Holes are drilled in the corrugated structure by placing the structure in between the moulds. The fabrication of double corrugated prototype is done by joining two single corrugated structures by means of rivets (flat head with 2 mm diameter). For riveting, one single corrugated structure is placed on top of the other and 3 rivets are punched along the width and along the length placed at every alternatively crest as shown in Fig. 17(b).

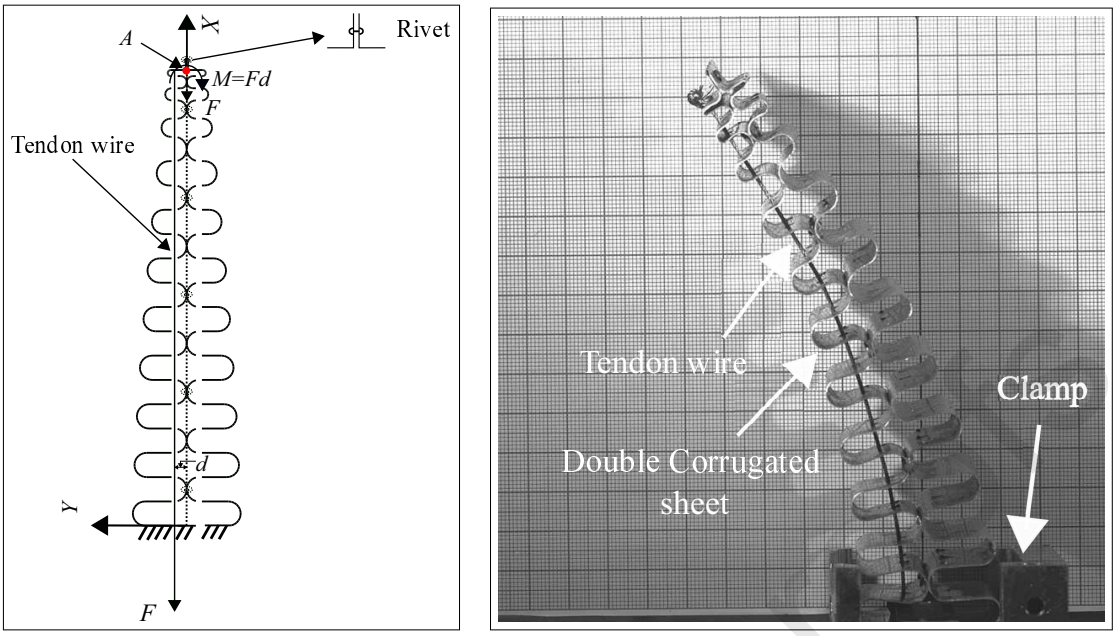

(a) (b)

Figure 18: Experimental setup for the tendon-load application (a) schematic representation, (b) deformed aluminum prototype under applied load.

Experimental setup for the tendon-load application on the double corrugated structure is shown in Fig. 18. For this experiment, the double corrugated structure prototype is clamped vertically on a vibration isolation table. The actuation force is applied through the spectra fiber wire (tendon) which is threaded through the holes and connected at the end of the structure. The diameter of the holes (0.2 mm) is made slightly larger than the wire diameter (0.1 mm), for smooth movement of the wire. Then known masses are suspended from the free end of the wire by using a load hanger to generate a known tension in the wire (F). The wire is connected with an offset of $d = 4mm$ *w.r.t.* to the center line of double corrugation (as shown in Fig. 18(a)). The offset in the wire connection produces an axial load (F) and equivalent moment ($M = Fd$) when shifted to point A located at center point of the end of double corrugation. In simulations, the effects of any interactions between wire and holes are not considered in this study. The displacements at tip of the aluminium corrugated sheet is measured using the digital photographs (Fig. 18(b)) for static load. The images are taken using a combination of point grey GS3-U3-41C6M sensor and TAMRON 180 mm 1:3.5 MACRO 1:1 lens.

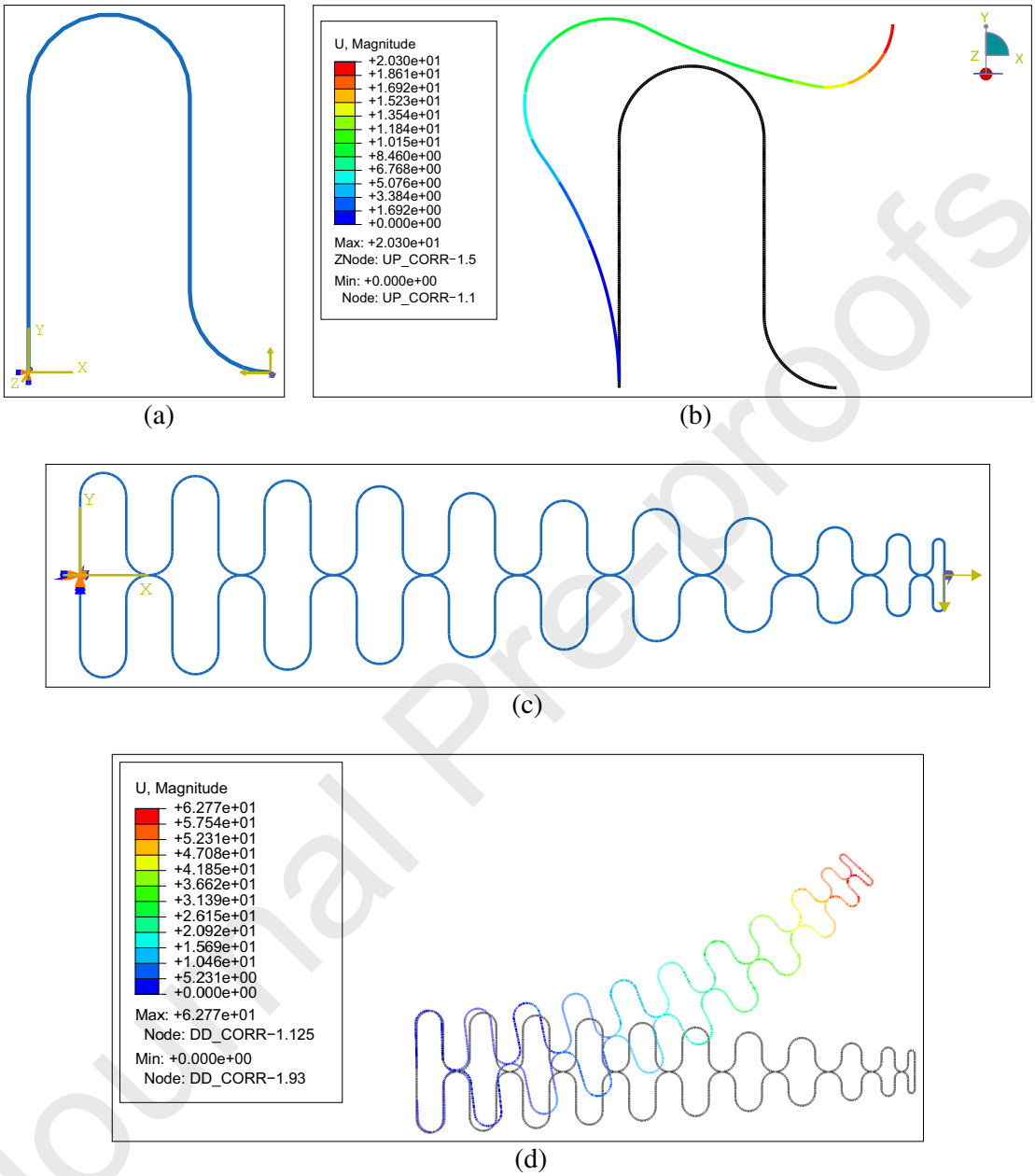

Figure 19: FEA models in ABAQUS® (a) Top open chain unit with the boundary conditions and the applied end loads, (b) deflected profile of top open chain unit due to the applied end loads (P_h = 50 N, P_v = 50 N, M_0 = 1000 N-mm), (c) double corrugated structure with the boundary conditions and the applied end loads, (d) deflected profile of double corrugated structure due to the applied end loads (P_h = −1 N, P_v = −2 N, M_0 = 1000 N-mm).

6. Results and discussion

Finite element models of the open chain unit, the basic corrugated unit and the double corrugated structure, considering geometric nonlinearity, are developed in ABAQUS® commercial software (see Fig. 19) [34]. A two noded in-plane Euler-Bernoulli beam element (B23 element) with cubic interpolation function is used for discretization. Figures 19(a) and (c) show the structure model of top open chain unit and double corrugated structure with boundary condition and applied end loads modeled in ABAQUS®. The deflected profiles of top open chain unit and double corrugated structure are shown in Figs. 19(b) and (d) for one particular set of applied end loads. Geometrical and material parameters considered for the analysis are given in Table 1. Linear elastic material behavior is considered in the analysis.

Convergence study

Computational cost and time play important role in choosing the type of element for numerical analysis. A convergence study has been done based on the same for the double corrugated structure model. Convergence criteria is given by Eq. 10 in which δ_1 and δ_2 are the tolerance values for the convergence of element size and load increment size respectively. $\delta_1 = \delta_2 = 10^{-4}$ are considered for the simulations and U is the magnitude of tip displacement. Fig. 20 (a) shows the element size and Fig. 20 (b) shows the load increment size convergence studies for the double corrugated structure. The results are plotted from element size 2 mm to 0.05 mm and load increment size from 0.05 to 0.005 in descending order to achieve convergence. From the study, it is observed that an element size of 0.1 mm and load increment size of 0.01 would provide good convergence.

$$\delta_1 = \frac{|U_{i+1} - U_i|}{U_i} \quad \text{and} \quad \delta_2 = \frac{|U_{j+1} - U_j|}{U_j} \tag{10}$$

Where U_i = Magnitude of tip displacement for the i^{th} element size ($i = 1, 2, ..., 7$) and U_j = Magnitude of tip displacement for the j^{th} load increment size ($j = 1, 2, ..., 7$).

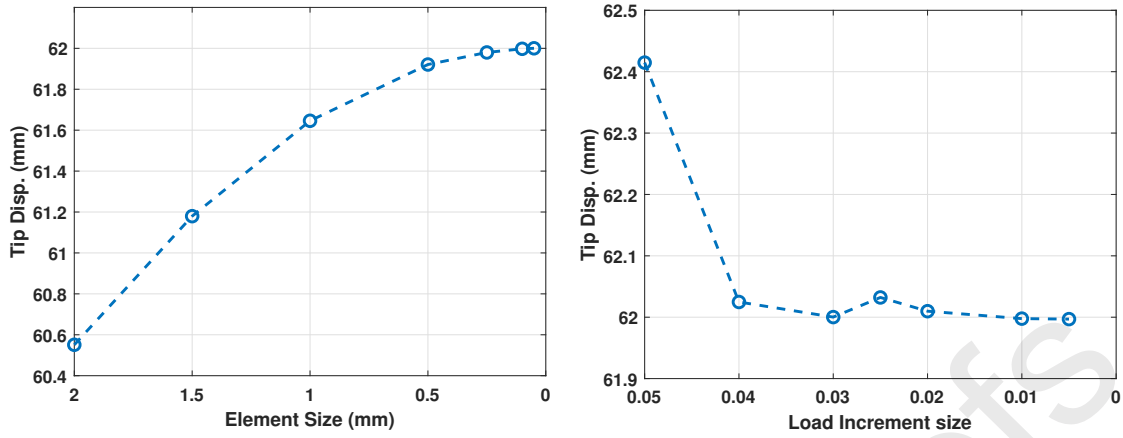

(a) (b)

Figure 20: Convergence study for double corrugated structure (a) Element Size, (b) load increment size.

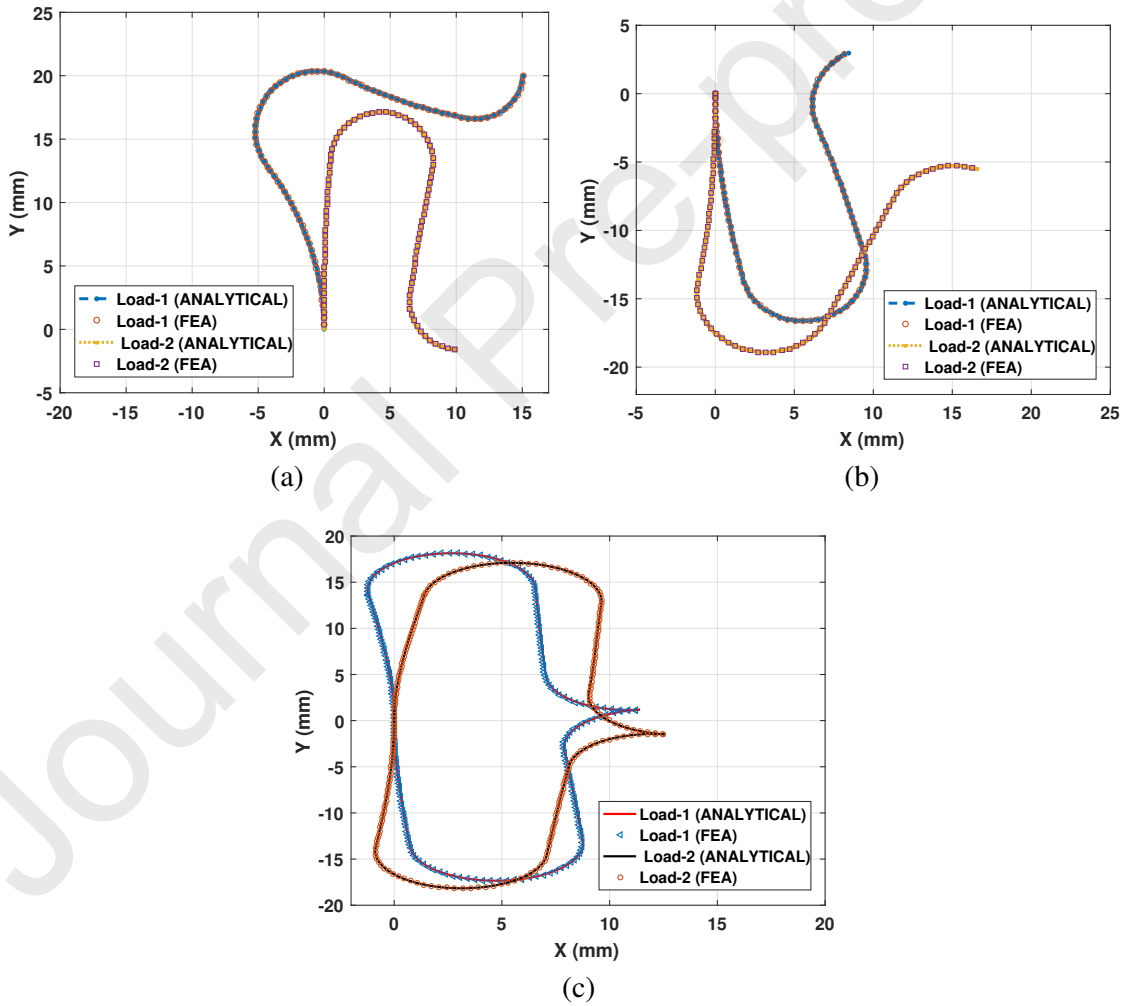

(a) (b)

(c)

Figure 21: Deflected profiles of the open chain units and the basic unit due to the applied end loads (a) top open chain unit, (b) bottom open chain unit and (c) basic corrugated unit.

6.1. *Open chain unit and the basic corrugated unit with cantilever boundary condition subjected to end point loads*

The results of the iterative scheme have been compared with the ABAQUS® solution for the open chain units and the basic corrugated unit due to applied end point loads. The deformed configurations of the open chain units and the basic corrugated unit due to the applied end point loads are shown in Figs. 21(a), (b) and (c) respectively. Two loading cases are considered for comparison-Load-1 and Load-2 as given in Table 4. The results obtained from the proposed model are found to be in good agreement with ABAQUS® for both the load cases.

Table 4: Loading parameters for the open chain units and the basic corrugated

	Load-1	Load-2
Top open chain unit	$P_h = 50$ N, $P_v = 50$ N, $M_0 = 1000$ N-mm	$P_h = 50$ N, $P_v = -100$ N, $M_0 = 1000$ N-mm
Bottom open chain unit	$P_h = -50$ N, $P_v = 50$ N, $M_0 = 1000$ N-mm	$P_h = -50$ N, $P_v = -100$ N, $M_0 = 1000$ N-mm
Basic corrugated unit	$P_h = 50$ N, $P_v = 50$ N, $M_0 = 1000$ N-mm	$P_h = -50$ N, $P_v = -75$ N, $M_0 = -1000$ N-mm

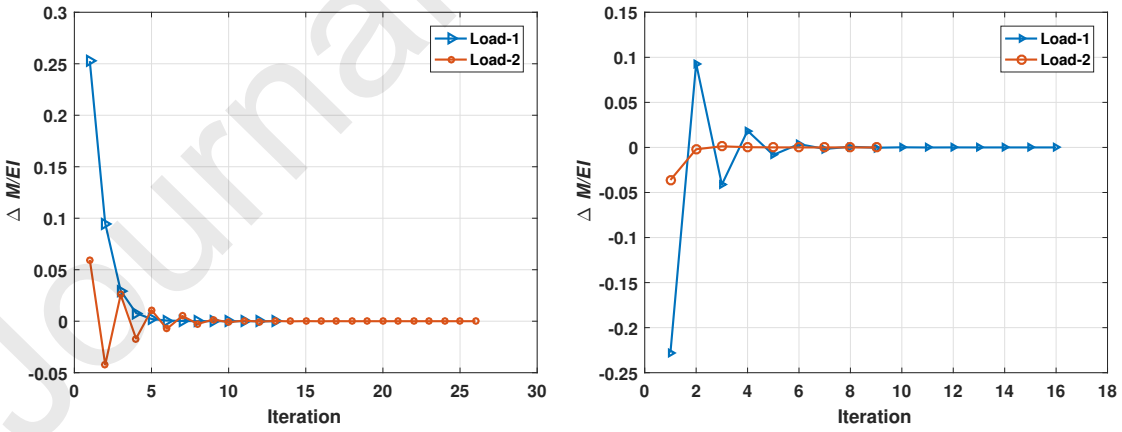

Figure 22: Convergence study using the chain algorithm. The moment variation ΔM for the node C and C' plotted against the number of iterations (a) top open chain unit, (b) bottom open chain unit.

Figures 22(a) and (b) show the convergence for the open chain units in which the variation of

the moment increment $\Delta M_j^i = M_j^i - M_{j-1}^i$ is plotted against the number of iterations for node C and C' in the top and bottom open chain unit respectively. For all load cases, the values of ΔM^C and $\Delta M^{C'}$ converge within 26 iterations.

In order to quantitatively assess the accuracy of the iterative scheme, the end point co-ordinates (x_{a_1}, y_{a_1}) obtained by the proposed method and that of the ABAQUS® are presented in Table 5. Error metrics, $\%E_x$ and $\%E_y$ are calculated as $\%E_x = \left|\frac{x_{iter}-x_{FEA}}{x_{iter}}\right|100$ and $\%E_y = \left|\frac{y_{iter}-y_{FEA}}{y_{iter}}\right|100$ as shown in Table 5 for the end point co-ordinates (x_{a_1}, y_{a_1}). The numerical results are obtained with a tolerance for the error metric, E_1 (Eq. (2)) as $10^{-4}\%$. In terms of prediction accuracy, it can be seen that the proposed iterative scheme shows excellent agreement with the ABAQUS® results. The error metrics, $\%E_x$ and $\%E_y$ are for all the cases are less than 2%.

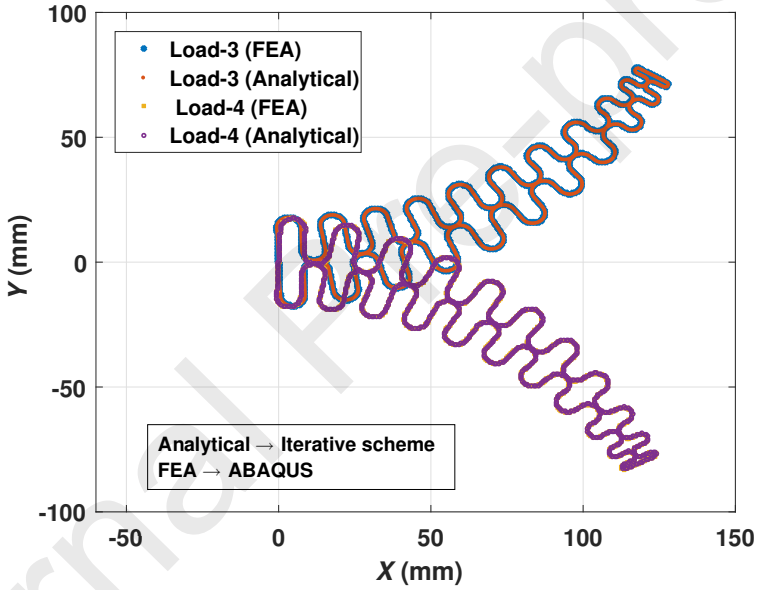

Figure 23: Deformed profiles of the double corrugated structure due to end loads.

6.2. Double corrugated structure with cantilever boundary condition subjected to end point loads

The deformed configurations of the double corrugated structure due to the applied end point loads are shown in Fig. 23. Two loading cases are considered for comparison-Load-3 and Load-4 as given in Table 6. The results obtained from the proposed model are found to be in good agreement with ABAQUS® for both the cases.

The response of the double corrugated structure, with loading conditions as given in Fig. 11,

Table 5: Comparison of solutions obtained using the iterative scheme and FEA (ABAQUS®) for the open chain units and the basic corrugated unit

Loads (Top open chain unit)	Iterative scheme		FEA (ABAQUS®)		$\%E_x = \left\lvert \frac{x_{iter} - x_{FEA}}{x_{iter}} \right\rvert 100$	
	x_{a_1} (mm)	y_{a_1} (mm)	x_{a_1} (mm)	y_{a_1} (mm)	$\%E_x$	$\%E_y$
$P_h = 50$ N, $P_v = 50$ N, $M_0 = 1000$ N-mm	15.0604	20.1038	15.1080	20.0654	0.3156	0.1913
$P_h = 50$ N, $P_v = -100$ N, $M_0 = 1000$ N-mm	9.9573	-1.6055	10.0037	-1.5843	0.4657	1.3197
$P_h = 50$ N, $P_v = 100$ N, $M_0 = 500$ N-mm	13.3614	23.8683	13.3634	23.8658	0.0144	0.0105
Loads (Bottom open chain unit)	Iterative scheme		FEA (ABAQUS®)		$\%E_x = \left\lvert \frac{x_{iter} - x_{FEA}}{x_{iter}} \right\rvert 100$	
	x_{a_1} (mm)	y_{a_1} (mm)	x_{a_1} (mm)	y_{a_1} (mm)	$\%E_x$	$\%E_y$
$P_h = -50$ N, $P_v = 50$ N, $M_0 = 1000$ N-mm	8.5087	3.0321	8.4754	3.0502	0.3919	0.5975
$P_h = -50$ N, $P_v = -100$ N, $M_0 = 1000$ N-mm	16.5939	-5.5385	16.5940	-5.5395	0.0004	0.0181
$P_h = 25$ N, $P_v = 25$ N, $M_0 = 1000$ N-mm	1.5352	2.82345	1.5373	2.8194	0.1358	0.1433
Loads (Basic corrugated unit)	Iterative scheme		FEA (ABAQUS®)		$\%E_x = \left\lvert \frac{x_{iter} - x_{FEA}}{x_{iter}} \right\rvert 100$	
	x_{a_1} (mm)	y_{a_1} (mm)	x_{a_1} (mm)	y_{a_1} (mm)	$\%E_x$	$\%E_y$
$P_h = 50$ N, $P_v = 50$ N, $M_0 = 1000$ N-mm	11.4096	1.1836	1.1985	0.05327	0.4131	1.2387
$P_h = -50$ N, $P_v = -75$ N, $M_0 = -1000$ N-mm	12.5941	-1.4903	12.6193	-1.5120	0.1994	1.4368
$P_h = 0$ N, $P_v = 0$ N, $M_0 = 1000$ N-mm	11.9882	0.6827	11.9773	0.6960	0.0917	1.9097

is shown in Fig. 24. The nonlinear behaviour can be seen in both the displacements, along x-axis (U_1) and along y-axis (U_2), for the proposed iterative scheme results, which is expected given

Table 6: Loading parameters for the double corrugated structure

Load-3	$P_h = 0$ N, $P_v = 0$ N, $M_0 = 1000$ N-mm
Load-4	$P_h = -1$ N, $P_v = -2$ N, $M_0 = -1000$ N-mm

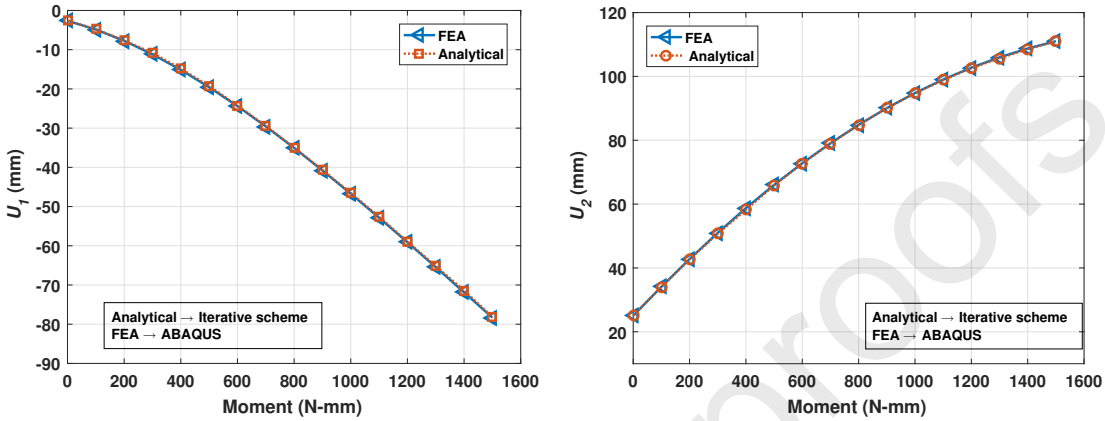

(a) (b)

Figure 24: Deflection at the tip (a_{11}) of the double corrugated structure under various end loads ($P_h = 2.5$ N and $P_v = 2.5$ N). (a) Displacement along x-axis (U_1), (b) displacement along y-axis (U_2).

the nonlinear nature of this formulation. ABAQUS® also predicts a nonlinear response over the applied moment range ($P_h = 2.5$ N and $P_v = 2.5$ N). In terms of prediction accuracy, it can be seen that the proposed iterative scheme shows excellent agreement with the ABAQUS® results. In the numerical studies, it is observed that the iterative scheme converges to the required solution atmost 1.15 times faster, in terms of computational time, than the ABAQUS® simulation without the loss of accuracy, as is evident from the results shown in Fig. 24.

6.3. Validation of the proposed iterative scheme with experiments

The experiments described in Section 3 use standard weights suspended at an eccentricity from the center of the double corrugated structure through a tendon wire as shown in Fig. 17. This tendon force produces an equivalent axial load and a moment about point A due to its eccentric attachment. These loads are applied in FE analysis and iterative scheme as shown in Fig. 25. The comparison of the force–displacement curve between the numerical, analytical and experimental results is shown in Fig. 26. Three prototypes made of aluminium with identical geometry as given in Table 1 are tested. The thickness of the fabricated double corrugated sheet is not constant due to

localised plastic deformation in the semi-circular sections. Therefore in FEA and iterative scheme model, thickness of corrugated sheets are given by measuring the sample thickness at semi-circular portion at different locations and the mean value is given as the thickness of entire structure.

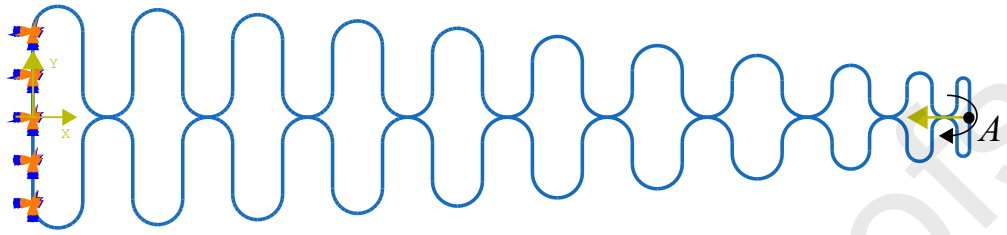

Figure 25: Double corrugated structure modeled using FEA in ABAQUS® with loading and boundary conditions to compare with experiments

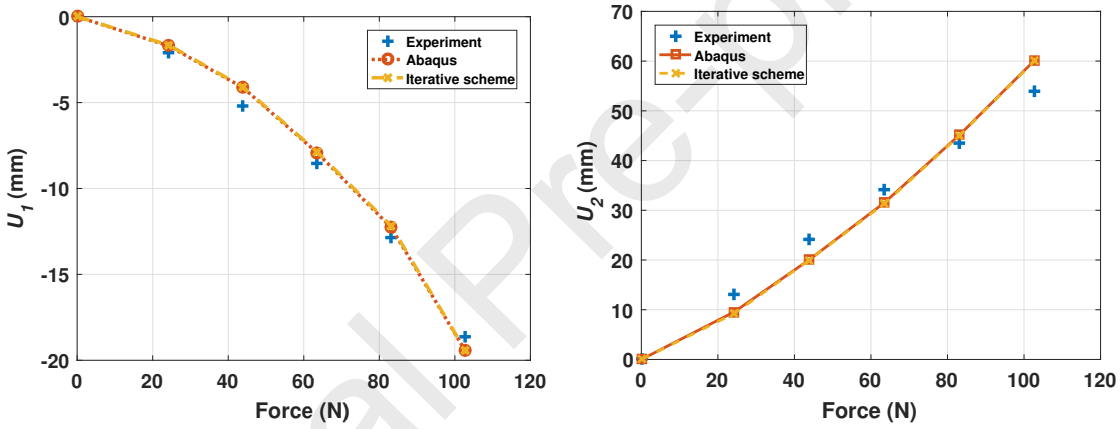

Figure 26: Deflection of the tip of the double corrugated structure under tendon force. (a) Displacement along x-axis (U_1), (b) displacement along y-axis (U_2).

Due to the large deformations, the force–displacement curve shows nonlinear variation with the applied load. Figures 26(a) and (b) compare the experimentally measured displacement along x-axis (U_1) and along y-axis (U_2) respectively, of the corrugated structure to that from the ABAQUS® and iterative scheme results. It can be seen from the Fig. 26, that results obtained from the ABAQUS® and the iterative scheme match closely to the results obtained from the experiments.

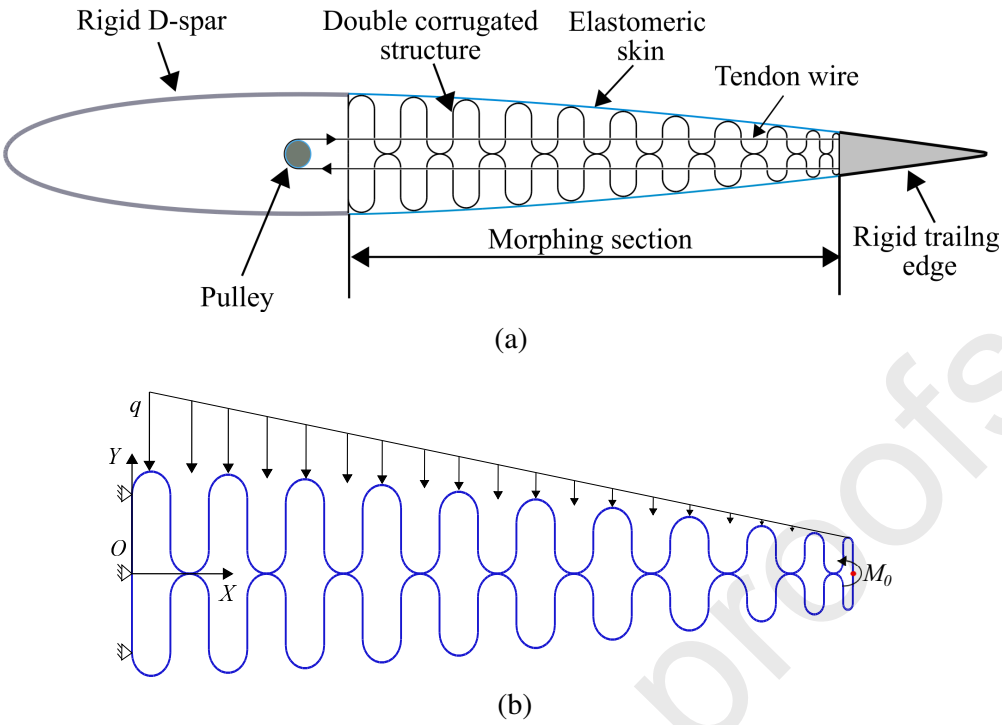

Figure 27: (a) Double corrugated variable camber morphing airfoil, (b) airfoil modeled as a cantilever double corrugated structure along with forces acting on it.

6.4. Practical application of the iterative scheme applied to a morphing structure

A novel concept of morphing wing with double corrugation has been proposed in Kumar et al. [7]. The proposed iterative scheme is applied to calculate the deflection of the morphing structure. As shown in Fig. 27 (a), the morphing wing consists of double corrugated structure as a core member which is connected to a elastomeric skin surface. The baseline shape of the wing is a symmetric NACA 0012 airfoil. The trailing edge of the morphing wing is actuated by actuators mounted in the rigid D-spar of the airfoil which drive a tendon spooling pulley system. Rotation of the pulley creates equal but opposite forces in tendons. These forces generate a bending moment on the trailing edge, thereby inducing bending of the trailing-edge morphing structure to create large changes in the airfoil camber.

The morphing wing is modeled as a cantilever double corrugated structure with an end moment as shown in Fig. 27(b). Furthermore, it is also subjected to a uniformly varying (triangular distribution) load, which results from the aerodynamic load [35] acting on the wing. The uniformly varying load has the peak value of q N/mm. For simplification only double corrugated structure is

Table 7: Loading parameters for double corrugated morphing wing

Load-5	q = 52.5 N/mm, M_0 = −750 N-mm
Load-6	q = 26.25 N/mm, M_0 = 750 N-mm

considered and the aerodynamic loads are applied directly to the semicircular segments and loads as concentrated forces. The concentrated forces are obtained as equivalent nodal forces. The problem defined is solved for different combination of loads as given in Table 4. The deflection of the double corrugated structure under the action of these forces, as shown in Fig. 27(b), is carried out using the proposed iterative scheme as given in Section 3. The results obtained for the two loading cases are shown in Fig. 28. Again, iterative scheme predicts the deflected profile with very high precision as compared with ABAQUS® simulations.

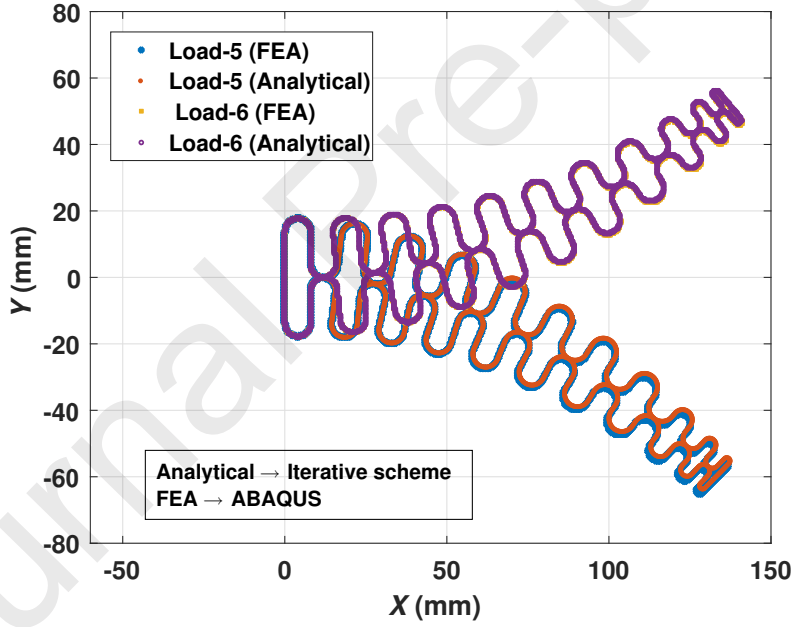

Figure 28: Deformed profiles of the double corrugated structure due to end loads.

7. Summary

In this paper, analytical, numerical and experimental studies on the large deflection of double corrugated cantilever structures are reported. Nonlinear shooting technique is integrated with a

chain algorithm in analytical solution. The deflections of a basic corrugated unit and a double corrugated structure are obtained using the proposed iterative scheme. Furthermore, prototypes of the corrugated structure are manufactured using aluminum sheets. The deflection of the prototypes is measured from photographs of the deformed structure. The deflected profile obtained from the iterative scheme is verified and compared with ABAQUS® and experiments. The results obtained from the iterative scheme are in close agreement with ABAQUS® while being substantially faster. There is a small difference in the values of the tip deflection obtained by the iterative scheme and ABAQUS® with experiments. The geometrical non-uniformity (localised plastic deformation due to riveting and fabricating process) and the residual stress developed due to the fabricating process of aluminum prototype could be possible reasons for the deviation of the iterative scheme and ABAQUS® results from experiments. The proposed method is capable of handling concentrated forces, distributed loads, concentrated moments thus providing reliable and versatile tool for catering to such complex geometry.

Future work can be focused on the development of iterative scheme for the double corrugated structure using composite material instead of aluminium for morphing application. However the implementation of composite material in our model poses the following challenges:

a. Composites have material nonlinearity while our model uses the linear elastic assumption.

b. Composite materials have direction dependent material properties [36, 37], hence it will be difficult to include in the current form of iterative scheme which is based on Euler-Bernoulli beam model.

c. Interface effect between two layers in a composite laminate is a challenging part to include in the current model.

Acknowledgment

The authors hereby acknowledge the funding obtained from DRDO (DRDO/DFTM/04/3304/PC /02/776/D (R&D)) through CoPT and ARDB (ARDB/01/1051810/M/I) projects.

References

[1] I. Dayyani, A. D. Shaw, E. I. S. Flores, M. I. Friswell, The mechanics of composite corrugated structures: a review with applications in morphing aircraft, Composite Structures 133 (2015) 358–380.

[2] A. Mukherjee, D. Kumar, S. F. Ali, A. Arockiarajan, Design and conception of a trailing edge morphing wing concept with bistable composite skin, in: Active and Passive Smart Structures and Integrated Systems XIV, Vol. 11376, SPIE, 2020, pp. 497 – 506.

[3] B. Cao, B. Hou, Y. Li, H. Zhao, An experimental study on the impact behavior of multilayer sandwich with corrugated cores, International Journal of Solids and Structures 109 (2017) 33 – 45.

[4] A. Mukherjee, S. F. Ali, A. Arockiarajan, Shape prediction of a composite wing panel under the action of an SMA wire and an MFC bimorph, in: Active and Passive Smart Structures and Integrated Systems XIII, Vol. 10967, SPIE, 2019, pp. 476 – 484.

[5] H. Takahashi, T. Yokozeki, Y. Hirano, Development of variable camber wing with morphing leading and trailing sections using corrugated structures, Journal of Intelligent Material Systems and Structures (2016) 1–10.

[6] H. Kalali, T. G. Ghazijahani, M. Hajsadeghi, T. Zirakian, F. J. Alaee, Numerical study on steel shear walls with sinusoidal corrugated plates, Latin American Journal of Solids and Structures 13 (15) (2016) 2802–2814.

[7] D. Kumar, S. F. Ali, A. Arockiarajan, Structural and aerodynamics studies on various wing configurations for morphing, IFAC-PapersOnLine 51 (2018) 498–503.

[8] D. Kumar, S. F. Ali, A. Arockiarajan, Studies on large deflection of geometrically nonlinear corrugated structure, Acta Mechanica 232 (2021) 461482.

[9] K. Dhileep, D. Kumar, S. Ghosh, S. Faruque Ali, A. Arockiarajan, Numerical study of camber morphing in NACA0012 airfoil, in: AIAA AVIATION Forum, Virtual event, 2020.

[10] J. T. Easley, D. E. McFarland, Buckling of light-gage corrugated metal shear diaphragms, Journal of the Structural Division 95 (7) (1969) 1497–1516.

[11] J. T. Easley, Buckling formulas for corrugated metal shear diaphragms, Journal of the structural Division 101 (7) (1975) 1403–1417.

[12] J. W. Berman, M. Bruneau, Experimental investigation of light-gauge steel plate shear walls, Journal of Structural Engineering 131 (2) (2005) 259–267.

[13] J. Z. Tong, Y. L. Guo, Shear resistance of stiffened steel corrugated shear walls, Thin-Walled Structures 127 (2018) 76–89.

[14] J. Z. Tong, Y. L. Guo, Elastic buckling behavior of steel trapezoidal corrugated shear walls with vertical stiffeners, Thin-Walled Structures 95 (2015) 31–39.

[15] J. Z. Tong, Y. L. Guo, J. Q. Zuo, Elastic buckling and load-resistant behaviors of double-corrugated-plate shear walls under pure in-plane shear loads, Thin-Walled Structures 130 (2018) 593–612.

[16] S. Barbarino, O. Bilgen, R. M. Ajaj, M. I. Friswell, D. J. Inman, A review of morphing aircraft, Journal of Intelligent Material Systems and Structures 22 (2011) 823–877.

[17] T. Yokozeki, S. I. Takeda, T. Ogasawara, T. Ishikawa, Mechanical properties of corrugated composites for candidate materials of flexible wing structures, Composites Part A: Applied Science and Manufacturing 37 (2006) 1578–1586.

[18] T. Yokozeki, A. Sugiura, Y. Hirano, Development of variable camber morphing airfoil using corrugated structure, Journal of Aircraft 51 (2014) 1–7.

[19] I. Dayyani, M. I. Friswell, E. I. S. Flores, A general super element for a curved beam, International Journal of Solids and Structures 51 (17) (2014) 2931–2939.

[20] C. Thill, J. Etches, I. Bond, K. Potter, P. Weaver, Composite corrugated structures for morphing wing skin applications, Smart Materials and Structures 19 (12) (2010) 124009.

[21] F. Previtali, A. F. Arrieta, P. Ermanni, Performance of a three-dimensional morphing wing and comparison with a conventional wing, AIAA journal 52 (10) (2014) 2101–2113.

[22] Y. Xia, M. I. Friswell, E. I. S. Flores, Equivalent models of corrugated panels, International Journal of Solids and Structures 49 (2012) 1453–1462.

[23] Z. Ye, V. L. Berdichevsky, W. Yu, An equivalent classical plate model of corrugated structures, International Journal of Solids and Structures 51 (11) (2014) 2073 – 2083.

[24] Y. Aoki, W. Maysenhlder, Experimental and numerical assessment of the equivalent-orthotropic-thin-plate model for bending of corrugated panels, International Journal of Solids and Structures 108 (2017) 11 – 23.

[25] S. Atashipour, M. Al-Emrani, A realistic model for transverse shear stiffness prediction of composite corrugated-core sandwich elements, International Journal of Solids and Structures 129 (2017) 1 – 17.

[26] V. Tavaf, S. Banerjee, Generalized analytical dispersion equations for guided Rayleigh-Lamb (RL) waves and shear horizontal (SH) waves in corrugated waveguides, International Journal of Solids and Structures 202 (2020) 75 – 86.

[27] J. Z. Tong, Y. L. Guo, J. Q. Zuo, J. K. Gao, Experimental and numerical study on shear resistant behavior of double-corrugated-plate shear walls, Thin-Walled Structures 147 (2020) 106485.

[28] F. Previtali, A. F. Arrieta, P. Ermanni, Double-walled corrugated structure for bending-stiff anisotropic morphing skins, Journal of intelligent material systems and structures 26 (5) (2015) 599–613.

[29] L. L. Howell, Compliant mechanisms, John Wiley & Sons, New York, NY, 2001.

[30] A. Mukherjee, S. F. Ali, A. Arockiarajan, Compliant structure under follower forces and any combined loading: Theoretical and experimental studies, International Journal of Mechanical Sciences 153-154 (2019) 75–82.

[31] MATLAB, Version 9.0.0.341360 (R2016a), The MathWorks Inc., Natick, Massachusetts, 2016.

[32] L. Ozdamar, M. Demirhan, E. Onbasioglu, Pre-search screening: A technique to improve search efficiency in global optimization, in: Frontiers in Global Optimization, Springer, 2004, pp. 437–455.

[33] J. Kaniowski, W. Wronicz, J. Jachimowicz, E. Szymczyk, Methods for FEM analysis of riveted joints of thin-walled aircraft structures within the imperja project, in: 25th Symposium of the International Committee on Aeronautical Fatigue (ICAF), Bridging the Gap between Theory and Operational Practice, Springer, Rotterdam, The Netherlands, 27-29 May 2009, pp. 939–967.

[34] ABAQUS Documentation, Version 6.13, Dassault Systèmes Simulia Corp., Providence, RI, USA, 2013.

[35] B. K. S. Woods, I. Dayyani, M. I. Friswell, Fluid/structure-interaction analysis of the fish-bone-active-camber morphing concept, Journal of Aircraft 52 (2015) 307–319.

[36] G. Kress, M. Winkler, Corrugated laminate homogenization model, Composite Structures 92 (2010) 795–810.

[37] G. Kress, D. Filipovic, An analytical nonlinear morphing model for corrugated laminates, Curved and Layered Structures 6 (1) (2019) 57–67.